INTERNATIONAL JOURNAL FOR NUMERICAL METHODS IN ENGINEERING
Int. J. Numer. Meth. Engng 2006; **67**:449–498
Published online 18 January 2006 in Wiley InterScience (www.interscience.wiley.com). DOI: 10.1002/nme.1637

A novel 'optimal' exponential-based integration algorithm for von-Mises plasticity with linear hardening: Theoretical analysis on yield consistency, accuracy, convergence and numerical investigations

E. Artioli[1,‡], F. Auricchio[2,3,*,†] and L. Beirão da Veiga[4,§]

[1]*D.I.S.T.A.R.T., Università di Bologna, V. le del Risorgimento 2, 40136 Bologna, Italy*
[2]*Dipartimento di Meccanica Strutturale, Università di Pavia, Via Ferrata 1, 27100 Pavia, Italy*
[3]*Istituto di Matematica Applicata e Tecnologie Informatiche del CNR, Via Ferrata 1, 27100 Pavia, Italy*
[4]*Dipartimento di Matematica 'F. Enriques', Università di Milano, Via Saldini 50, 20133 Milano, Italy*

SUMMARY

In this communication we propose a new exponential-based integration algorithm for associative von-Mises plasticity with linear isotropic and kinematic hardening, which follows the ones presented by the authors in previous papers. In the first part of the work we develop a theoretical analysis on the numerical properties of the developed exponential-based schemes and, in particular, we address the yield consistency, exactness under proportional loading, accuracy and stability of the methods. In the second part of the contribution, we show a detailed numerical comparison between the new exponential-based method and two classical radial return map methods, based on backward Euler and midpoint integration rules, respectively. The developed tests include pointwise stress–strain loading histories, iso-error maps and global boundary value problems. The theoretical and numerical results reveal the optimal properties of the proposed scheme. Copyright © 2006 John Wiley & Sons, Ltd.

KEY WORDS: plasticity; exponential integration algorithm; return map; exact integration; integration factor

1. INTRODUCTION

The present paper constitutes the latest contribution by the authors to a series of previous communications regarding the development of a new class of exponential-based integration algorithms for von-Mises plasticity with linear isotropic and kinematic hardening.

*Correspondence to: F. Auricchio, Dipartimento di Meccanica Strutturale, Università di Pavia, Via Ferrata 1, 27100 Pavia, Italy.
†E-mail: auricchio@unipv.it
‡E-mail: artioli@imati.cnr.it
§E-mail: beirao@mat.unimi.it

Received 3 May 2005
Accepted 27 November 2005

There are several aims to this work. First, we introduce a modified time-continuous reformulation for the model under consideration based on a different choice for a generalized stress vector and for an integration factor. Then we present the corresponding integration scheme (ESC^2 scheme) for the reformulated differential-algebraic problem which makes use of exponential maps. The new scheme represents an improved evolution of other exponential-based integration procedures [1, 2]. We propose a thorough discussion on the consistency, accuracy and stability of the new numerical method from the analytical point of view.

Finally, we test the new scheme on a wide set of numerical examples. As a comparison, we adopt two classical radial return map-type methods based on two different integration rules. The first one is based on a backward Euler integration rule and it will be referred as RM method [3–5], while the second is based on a midpoint integration scheme and will be labelled as MPT [6]. To this end, also the previously developed exponential-based algorithms ENN, ENC and ESC (see References [1, 2] for details) are taken into account to show the improvements gained by the new scheme.

The present paper is organized as follows.

In Section 2 we introduce the basic equations governing the plasticity model under consideration, while in Section 3 we briefly recall a reformulation of the problem already presented in Reference [2]. The new formulation results in a quasi-linear form which is suitable for an effective step-by-step numerical integration using exponential maps. In Section 4 we present two numerical algorithms which stem from the preceding formulation. The first method is the ESC scheme already proposed in Reference [2], while the second one is the new 'optimal' ESC^2 algorithm.

In Section 5 we develop a theoretical analysis of the exponential methods presented by the authors here and in previous communications. First we address properties which are directly related to the plasticity problem, namely yield consistency, exactness in the absence of isotropic hardening and exactness under proportional loading. Afterwards, we address general properties in the analysis of numerical schemes for differential equations, namely accuracy and stability. In Section 6, we undertake a wide testing of the ESC and ESC^2 methods considering piecewise stress–strain load histories, iso-error maps and boundary value problems. The numerical investigations are expressed in terms of solution accuracy and Newton convergence speed, comparing both exponential-based schemes also with the classical radial return map integration schemes based either on backward Euler or midpoint integration rules.

Differently from the ESC scheme, the results of Section 6 show that the ESC^2 method is quadratically accurate and exact under proportional load histories. Moreover, the improved performance of the ESC^2 scheme using large time steps is clearly appreciable when a direct comparison is made with the other tested methods by means of iso-error maps. In this sense, the new ESC^2 procedure is 'optimal', since it grants specific features that makes it the most competitive within the exponential-based set family.

Finally, in Appendix A, we present two technical lemmas and a complete detailed derivation of the algorithmically consistent tangent operators both for the ESC and ESC^2 algorithms.

Remark 1.1

Throughout the whole paper we adopt a compact matrix notation. Accordingly, all second rank and fourth rank symmetric tensors are indicated by 6×1 column vectors and 6×6 symmetric matrices. The definition of trace and Euclidean norm are consequently modified.

2. TIME CONTINUOUS MODEL

We consider an associative von-Mises plasticity model with linear kinematic and isotropic hardening in the realm of small deformations (refer for example to References [7, 8] or [9]). Splitting the strain and stress vectors, $\boldsymbol{\sigma}$ and $\boldsymbol{\varepsilon}$, in deviatoric and volumetric parts we have

$$\boldsymbol{\sigma} = \mathbf{s} + p\mathbf{i} \quad \text{with} \quad p = \tfrac{1}{3}\mathrm{tr}(\boldsymbol{\sigma}) \tag{1}$$

$$\boldsymbol{\varepsilon} = \mathbf{e} + \tfrac{1}{3}\theta\mathbf{i} \quad \text{with} \quad \theta = \mathrm{tr}(\boldsymbol{\varepsilon}) \tag{2}$$

where tr indicates the trace operator (sum of the first three components), while $\mathbf{i}$, $\mathbf{s}$, p, $\mathbf{e}$, θ are, respectively, the vector corresponding to the second rank identity tensor, the deviatoric and volumetric stresses, the deviatoric and volumetric strains.

The equations for the model are

$$p = K\theta \tag{3}$$

$$\mathbf{s} = 2G[\mathbf{e} - \mathbf{e}^{\mathrm{p}}] \tag{4}$$

$$\boldsymbol{\Sigma} = \mathbf{s} - \boldsymbol{\alpha} \tag{5}$$

$$F = \|\boldsymbol{\Sigma}\| - \sigma_{\mathrm{y}} \tag{6}$$

$$\dot{\mathbf{e}}^{\mathrm{p}} = \dot{\gamma}\mathbf{n} \tag{7}$$

$$\sigma_{\mathrm{y}} = \sigma_{\mathrm{y},0} + H_{\mathrm{iso}}\gamma \tag{8}$$

$$\dot{\boldsymbol{\alpha}} = H_{\mathrm{kin}}\dot{\mathbf{e}}^{\mathrm{p}} \tag{9}$$

$$\dot{\gamma} \geqslant 0, \quad F \leqslant 0, \quad \dot{\gamma}F = 0 \tag{10}$$

where K is the material bulk elastic modulus, G is the material shear modulus, $\mathbf{e}^{\mathrm{p}}$ is the traceless plastic strain, $\boldsymbol{\Sigma}$ is the relative stress in terms of the backstress $\boldsymbol{\alpha}$, the latter introduced to describe a kinematic hardening mechanism. Moreover, F is the von-Mises yield function, $\mathbf{n}$ is the normal to the yield surface, σ_{y} is the yield surface radius, $\sigma_{\mathrm{y},0}$ the initial yield stress, H_{kin} and H_{iso} are the kinematic and isotropic hardening moduli. Finally, Equations (10) are the Kuhn–Tucker conditions; in particular, the second equation limits the relative stress within the boundary defined by the yield surface $F = 0$, while the other two are necessary to determine the plastic behaviour. With a slight over-simplification of the model complexity, we may say that when $\dot{\gamma} = 0$ the system is in an elastic phase, while when $\dot{\gamma} > 0$ we say that the system is in a plastic phase.

Remark 2.1
Due to the linear behaviour of the volumetric part constitutive equations, we treat only the deviatoric part of the model.

3. A NEW MODEL FORMULATION

In this section we present a new time-continuous model formulation for the differential algebraic problem under consideration. This innovative statement of the problem represents

a generalization of the formulation presented in References [2, 10] and thus constitutes an extension of the ones proposed in References [1, 11, 12]. Such a formulation allows to rewrite the system in the form

$$\dot{\mathbf{X}} = \mathbb{A}\mathbf{X} \tag{11}$$

which is the starting point for the numerical scheme developed in Section 4.

Combining Equations (4) and (5), we obtain

$$\boldsymbol{\Sigma} + \boldsymbol{\alpha} + 2G\mathbf{e}^{\mathrm{p}} = 2G\mathbf{e} \tag{12}$$

which, taking the derivative in time, applying Equation (9) and rearranging terms gives

$$\dot{\boldsymbol{\Sigma}} = 2G\dot{\mathbf{e}} - (2G + H_{\mathrm{kin}})\dot{\mathbf{e}}^{\mathrm{p}} \tag{13}$$

Now, recalling the yield surface radius

$$\sigma_{\mathrm{y}} = \sigma_{\mathrm{y},0} + H_{\mathrm{iso}}\gamma \tag{14}$$

and that in the plastic phase

$$\mathbf{n} = \frac{\boldsymbol{\Sigma}}{\|\boldsymbol{\Sigma}\|} = \frac{\boldsymbol{\Sigma}}{\sigma_{\mathrm{y},0} + H_{\mathrm{iso}}\gamma} = \frac{\boldsymbol{\Sigma}}{\sigma_{\mathrm{y}}} \tag{15}$$

we may apply (7) obtaining

$$\dot{\boldsymbol{\Sigma}} + (2G + H_{\mathrm{kin}})\frac{\boldsymbol{\Sigma}}{\sigma_{\mathrm{y}}}\dot{\gamma} = 2G\dot{\mathbf{e}} \tag{16}$$

which is a differential equation for $\boldsymbol{\Sigma}$ that is valid also during elastic phases ($\dot{\gamma} = 0$). Introducing the *scaled relative stress*

$$\bar{\boldsymbol{\Sigma}} = \frac{\boldsymbol{\Sigma}}{\sigma_{\mathrm{y}}} \tag{17}$$

we observe that, whenever the relative stress $\boldsymbol{\Sigma}$ lays on the yield surface, then $\bar{\boldsymbol{\Sigma}} = \mathbf{n}$, while this is not true when $\boldsymbol{\Sigma}$ lays inside the yield surface. The time derivative of (17) and the use of relation (14) gives

$$\dot{\bar{\boldsymbol{\Sigma}}} = \frac{\dot{\boldsymbol{\Sigma}}}{\sigma_{\mathrm{y}}} - \frac{H_{\mathrm{iso}}}{\sigma_{\mathrm{y}}}\dot{\gamma}\bar{\boldsymbol{\Sigma}} \tag{18}$$

Dividing Equation (16) by σ_{y} and using relationship (18), one obtains

$$\dot{\bar{\boldsymbol{\Sigma}}} + \frac{2G + H_{\mathrm{kin}} + H_{\mathrm{iso}}}{\sigma_{\mathrm{y}}}\dot{\gamma}\bar{\boldsymbol{\Sigma}} = \frac{2G}{\sigma_{\mathrm{y}}}\dot{\mathbf{e}} \tag{19}$$

The next goal is to introduce an *integration factor* for the above evolutionary equation.

Accordingly, we set

$$X_0(\gamma) = \begin{cases} \left(1 + \dfrac{\gamma H_{\text{iso}}}{\sigma_{\text{y},0}}\right)^{2G+H_{\text{kin}}+H_{\text{iso}}/H_{\text{iso}}} & \text{if } H_{\text{iso}} \neq 0 \\ \exp\left(\dfrac{2G + H_{\text{kin}} + H_{\text{iso}}}{\sigma_{\text{y},0}}\gamma\right) & \text{if } H_{\text{iso}} = 0 \end{cases} \tag{20}$$

noting that such a function is continuous for fixed γ and $H_{\text{iso}} \to 0$ and that

$$\dot{X}_0 = \frac{2G + H_{\text{kin}} + H_{\text{iso}}}{\sigma_{\text{y}}}\dot{\gamma}X_0 \tag{21}$$

Multiplying Equation (19) by X_0 and using Equation (21) the following relationship holds:

$$\frac{\mathrm{d}}{\mathrm{d}t}[X_0\bar{\boldsymbol{\Sigma}}] = X_0\dot{\bar{\boldsymbol{\Sigma}}} + \dot{X}_0\bar{\boldsymbol{\Sigma}} = \frac{2G}{\sigma_{\text{y}}}X_0\dot{\mathbf{e}} \tag{22}$$

At this stage, defining a new 7-dimensional *generalized stress vector* $\mathbf{X}$ as

$$\mathbf{X} = \begin{pmatrix} X_0\bar{\boldsymbol{\Sigma}} \\ X_0 \end{pmatrix} = \begin{pmatrix} \mathbf{X}^{\text{s}} \\ X_0 \end{pmatrix} \tag{23}$$

Equation (22) can be rewritten as

$$\dot{\mathbf{X}}^{\text{s}} = \frac{2G}{\sigma_{\text{y}}}X_0\dot{\mathbf{e}} \tag{24}$$

The evolution law for X_0 in terms of $\mathbf{X}$ in elastic phases follows immediately from (21)

$$\dot{X}_0 = 0 \quad \text{(elastic phases)} \tag{25}$$

On the other hand, for $\dot{\gamma} \neq 0$, taking the scalar product of (22) with $\bar{\boldsymbol{\Sigma}}$, we have

$$X_0\frac{1}{2}\frac{\mathrm{d}}{\mathrm{d}t}\|\bar{\boldsymbol{\Sigma}}\|^2 + \dot{X}_0\|\bar{\boldsymbol{\Sigma}}\|^2 = \frac{2G}{\sigma_{\text{y}}}X_0\dot{\mathbf{e}} \cdot \bar{\boldsymbol{\Sigma}} \tag{26}$$

which, noting that in plastic phases

$$\|\bar{\boldsymbol{\Sigma}}\| = \frac{\|\boldsymbol{\Sigma}\|}{\sigma_{\text{y}}} = 1 \tag{27}$$

and using (23), (26) gives

$$\dot{X}_0 = \frac{2G}{\sigma_{\text{y}}}\dot{\mathbf{e}} \cdot \mathbf{X}^{\text{s}} \quad \text{(plastic phases)} \tag{28}$$

Equations (24), (25) and (28) provide a system for the *generalized stress vector* $\mathbf{X}$, in the form

$$\dot{\mathbf{X}} = \mathbb{A}\mathbf{X} \tag{29}$$

with the matrix $\mathbb{A}$ depending on the actual phase as follows:

$$\mathbb{A} = \frac{2G}{\sigma_y} \begin{pmatrix} 0_{6\times 6} & \dot{\mathbf{e}} \\ 0_{1\times 6} & 0 \end{pmatrix} \quad \text{(elastic phase)} \tag{30}$$

$$\mathbb{A} = \frac{2G}{\sigma_y} \begin{pmatrix} 0_{6\times 6} & \dot{\mathbf{e}} \\ \dot{\mathbf{e}}^T & 0 \end{pmatrix} \quad \text{(plastic phase)} \tag{31}$$

and with $\mathbb{A}$ symmetric during plastic phases. Therefore the original problem, expressed by Equations (4)–(9), has been substituted by a new one, expressed by Equations (29)–(31).

We also observe that in the case of no isotropic hardening ($H_{\text{iso}} = 0$) the yield radius σ_y is fixed and therefore $\mathbb{A}$ depends only on $\dot{\mathbf{e}}$. This means that, if $\dot{\mathbf{e}}$ is constant in a given time interval, $\mathbb{A}$ holds the same property: under such an hypothesis the solution of system (29) is known and the problem can be solved exactly.

However, in a general case ($H_{\text{iso}} \neq 0$) the matrix $\mathbb{A}$ depends on $\mathbf{X}$ and in this sense we say that the problem is 'quasi linear'. Anyway, the 'quasi linearity' arising in the problem is indeed of great value, allowing us to develop the numerical method of Section 4.

3.1. Time-continuous on--off switch

To properly convert the original problem in a new but equivalent differential algebraic format, we also need to introduce an elasto-plastic phase determination criterium expressed in the new generalized stress environment.

For a given state to be plastic, the following two conditions must be fulfilled:

(1) The relative stress $\boldsymbol{\Sigma}$ must be on the yield surface, in other words

$$\|\boldsymbol{\Sigma}\| = \sigma_y \tag{32}$$

Using (17) and (23) this can be easily rewritten as

$$\|\mathbf{X}^s\|^2 = \|\bar{\boldsymbol{\Sigma}}\|^2 X_0^2 = \frac{\|\boldsymbol{\Sigma}\|^2}{\sigma_y^2} X_0^2 = X_0^2 \tag{33}$$

(2) The direction of the strain rate $\dot{\mathbf{e}}$ must be outward with respect to the yield surface, i.e.

$$\boldsymbol{\Sigma} \cdot \dot{\mathbf{e}} > 0 \tag{34}$$

Again, recalling (17) and (23) it is immediate to check that (34) is equivalent to

$$\mathbf{X}^s \cdot \dot{\mathbf{e}} > 0 \tag{35}$$

If the two conditions (33) and (35) are not satisfied, the step is elastic.

4. NUMERICAL SCHEME

We now want to develop a numerical scheme for the evolution of $\mathbf{X}$, governed by the dynamical law (29) with matrix $\mathbb{A}$ given by (30) or (31), respectively.

4.1. Time integration procedure

As usual, we assume that the time history interval $[0, T]$ is divided into N sub-intervals defined by the nodes $0 = t_0 < t_1 < \cdots < t_n < t_{n+1} < \cdots < t_N = T$ and indicate the general sub-interval amplitude as $\Delta t = t_{n+1} - t_n$. Given the values $(\mathbf{s}_n, \mathbf{e}_n, \gamma_n, \boldsymbol{\alpha}_n)$ at time t_n and the deviatoric strain $\mathbf{e}_{n+1}$ at time t_{n+1}, we search for the remaining variables at time t_{n+1}, assuming the strain history to be piecewise linear. For simplicity, we consider the initial values (at $t = t_0$) of $\gamma, \mathbf{e}^{\mathrm{p}}$ and $\boldsymbol{\alpha}$ to be zero, so that the initial *generalized stress vector* is

$$\mathbf{X}_0 = \begin{pmatrix} \boldsymbol{\Sigma}_0 / \sigma_{\mathrm{y},0} \\ 1 \end{pmatrix} \tag{36}$$

Due to the piecewise linearity of the strain path, $\dot{\mathbf{e}}$ is constant in each single time interval. Unluckily, due to the presence of σ_{y} in (31), during plastic phases, the matrix $\mathbb{A}$ is not constant in the same time interval; in fact the yield surface radius σ_{y} is a function of X_0, as shown by relation (21) and hence of $\mathbf{X}$. Therefore, we discretize the dynamical law (29), approximating σ_{y} as stepwise. Along each time interval $[t_n, t_{n+1}]$, we choose $\sigma_{\mathrm{y}} = R$, where R is now a constant value in each single time step. It is evident that for purely elastic steps the R value coincides with $\sigma_{\mathrm{y},n}$. The discrete form of the evolution law (29) becomes

$$\dot{\mathbf{X}} = \bar{\mathbb{A}} \mathbf{X} \tag{37}$$

where the matrix $\bar{\mathbb{A}}$ is now constant along a single time interval

$$\bar{\mathbb{A}} = \frac{2G}{\sigma_{\mathrm{y},n}} \begin{pmatrix} 0_{6\times 6} & \dot{\mathbf{e}} \\ 0_{1\times 6} & 0 \end{pmatrix} \quad \text{(elastic phase)} \tag{38}$$

$$\bar{\mathbb{A}} = \frac{2G}{R} \begin{pmatrix} 0_{6\times 6} & \dot{\mathbf{e}} \\ \dot{\mathbf{e}}^{\mathrm{T}} & 0 \end{pmatrix} \quad \text{(plastic phase)} \tag{39}$$

Different choices for R are clearly possible, for example

$$\begin{aligned} R &= \sigma_{\mathrm{y},n} \quad \text{(ESC scheme)} \\ R &= \frac{c\sigma_{\mathrm{y},n}}{\ln(1+c)} \quad \text{(ESC}^2\text{ scheme)} \end{aligned} \tag{40}$$

where

$$c = \frac{2Gq(1-\alpha)\left(\dfrac{\mathbf{X}_n^{\mathrm{s}}}{X_{0,n}} \cdot \dot{\mathbf{e}}\right)}{\sigma_{\mathrm{y},n}} \Delta t \tag{41}$$

with

$$q = \frac{H_{\mathrm{iso}}}{2G + H_{\mathrm{kin}} + H_{\mathrm{iso}}} \tag{42}$$

The α scalar parameter represents the part of the step along which the stress vector remains within the limit surface (see Figure 1(a)). Its calculation will be explained and discussed in detail in Section 4.2 for compactness reasons.

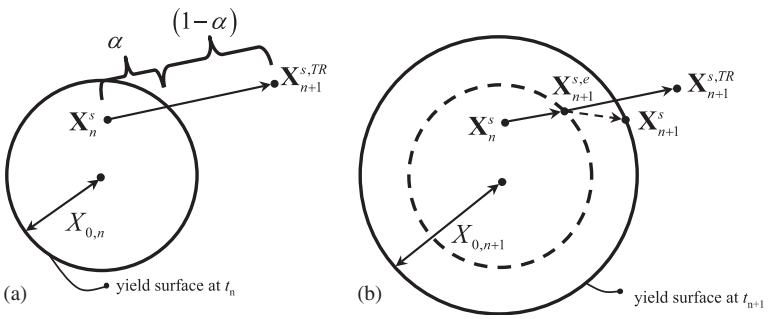

Figure 1. Exponential-based schemes update procedure in the generalized relative stress space during a mixed elasto-plastic step.

The first choice for R in (40) corresponds to the ESC scheme already proposed in Reference [2], the second one leads to the new ESC^2 scheme which is the object of the present paper. While the reasonings for the first choice for R are evident ('forward integration' scheme), the second choice for R comes from considerations regarding the improved numerical properties of the new exponential-based algorithm, discussed from the analytical standpoint in Section 5.

Due to the fact that R is computed using only quantities evaluated at the beginning of the step, the matrix $\bar{\mathbb{A}}$ is now constant in both elastic and plastic phases and so Equation (37) can be solved exactly, giving the following evolution for $\mathbf{X}$:

$$\mathbf{X}_{n+1} = \exp\left[\bar{\mathbb{A}}\Delta t\right]\mathbf{X}_n = \bar{\mathbb{G}}\mathbf{X}_n \tag{43}$$

Defining the vector $\Delta\mathbf{e} = \mathbf{e}_{n+1} - \mathbf{e}_n$, we observe that the matrix $\bar{\mathbb{A}}\Delta t$ is equal to the matrix (38) or (39) after substituting $\dot{\mathbf{e}}$ with $\Delta\mathbf{e}$.

Therefore, the matrix $\bar{\mathbb{G}}$ is

$$\bar{\mathbb{G}} = \begin{cases} \bar{\mathbb{G}}_{\mathrm{e}} = \begin{pmatrix} \mathbb{I} & \dfrac{2G}{\sigma_{\mathrm{y},n}}\Delta\mathbf{e} \\ 0 & 1 \end{pmatrix} & \text{(elastic phase)} \\ \bar{\mathbb{G}}_{\mathrm{p}} = \begin{pmatrix} \mathbb{I} + \left[\dfrac{(a-1)}{\|\Delta\mathbf{e}\|^2}\right]\Delta\mathbf{e}\Delta\mathbf{e}^{\mathrm{T}} & b\dfrac{\Delta\mathbf{e}}{\|\Delta\mathbf{e}\|} \\ b\dfrac{\Delta\mathbf{e}^{\mathrm{T}}}{\|\Delta\mathbf{e}\|} & a \end{pmatrix} & \text{(plastic phase)} \end{cases} \tag{44}$$

where the scalars a and b are

$$a = \cosh\left(\frac{2G}{R}\|\Delta\mathbf{e}\|\right) \tag{45}$$

$$b = \sinh\left(\frac{2G}{R}\|\Delta\mathbf{e}\|\right) \tag{46}$$

and where $\mathbb{I}$ is the 6×6 identity matrix.

4.2. Solution algorithm

At every time step the exponential-based algorithm proceeds as follows:

(1) Suppose the step to be elastic and compute trial values following an elastic law:

$$\mathbf{X}_{n+1}^{\mathrm{TR}} = \bar{\mathbb{G}}_{\mathrm{e}} \mathbf{X}_n \tag{47}$$

where the matrix $\bar{\mathbb{G}}_{\mathrm{e}}$ is given by (44). If the trial solution is admissible, i.e.

$$\|\mathbf{X}_{n+1}^{\mathrm{s,TR}}\| \leqslant (X_{0,n+1}^{\mathrm{TR}})^2 \tag{48}$$

then the variable values at the time step t_{n+1} are taken as the trial ones just calculated.

(2) If the trial solution is non-admissible, i.e. Equation (48) is violated, then the step is plastic or elasto-plastic. Being $\dot{\mathbf{e}}$ constant in each time sub interval, the step can be divided into two parts: an elastic deformation taking place during $[t_n, t_{n+\alpha}]$, followed by a plastic one along $[t_{n+\alpha}, t_{n+1}]$. Hence, we represent with a scalar $\alpha \in [0, 1)$ the elastic time proportion of the step. The key consideration in order to calculate α is that the evolution during the partial elastic sub-step is linear in stress space. Accordingly, recalling (44), we search for an intermediate generalized stress vector

$$\mathbf{X}_{n+1}^{\mathrm{s,e}} = \mathbf{X}_n^{\mathrm{s}} + \frac{2GX_{0,n}}{\sigma_{\mathrm{y},n}}[\alpha \Delta \mathbf{e}] \tag{49}$$

such that $\mathbf{X}_{n+1}^{\mathrm{s,e}}$ represents a stress vector lying on the yield surface at time $t_{n+\alpha}$. In other words, we must request

$$\mathbf{X}_{n+1}^{\mathrm{s,e}} \cdot \mathbf{X}_{n+1}^{\mathrm{s,e}} - X_{0,n}^2 = 0 \tag{50}$$

Note that the left-hand side of the above equation is a second-order polynomial in α. In stress space, the roots of such polynomial correspond to the intersections between a segment and the boundary of a sphere, where an extreme of the segment ($\mathbf{s}_n$) lays inside the sphere closure and the other extreme ($\mathbf{s}_n + 2G\Delta\mathbf{e}$) outside the sphere. As a consequence there is always one maximum (non-negative) root. Calculating therefore α from expression (50) we get

$$\alpha = \frac{\sqrt{C^2 - DM} - C}{D} \tag{51}$$

where

$$\begin{aligned} C &= \frac{2GX_{0,n}}{\sigma_{\mathrm{y},n}}(\mathbf{X}_n^{\mathrm{s}} \cdot \Delta\mathbf{e}) \\ D &= \left(\frac{2GX_{0,n}\|\Delta\mathbf{e}\|}{\sigma_{\mathrm{y},n}}\right)^2 \\ M &= \|\mathbf{X}_n^{\mathrm{s}}\|^2 - (X_{0,n+1}^{\mathrm{TR}})^2 \end{aligned} \tag{52}$$

Computed α, $\mathbf{X}_{n+1}$ is updated in two steps:

— Calculate a new $\mathbf{X}^{\mathrm{e}}_{n+1}$ vector following an elastic law along an $\alpha\Delta t$ interval:

$$\mathbf{X}^{\mathrm{e}}_{n+1} = \bar{\mathbb{G}}_{\mathrm{e}}[\alpha\Delta\mathbf{e}]\mathbf{X}_n \tag{53}$$

— Calculate $\mathbf{X}_{n+1}$ evolving from the new initial data $\mathbf{X}^{\mathrm{e}}_{n+1}$ following a plastic law along the remaining part of the interval of amplitude $(1-\alpha)\Delta t$

$$\mathbf{X}_{n+1} = \bar{\mathbb{G}}_{\mathrm{p}}[(1-\alpha)\Delta\mathbf{e}]\mathbf{X}^{\mathrm{e}}_{n+1} \tag{54}$$

Observe that in such a framework purely plastic steps are simply those where the time proportion of the elastic phase α is zero.

(3) Update the yield surface radius

$$\sigma_{\mathrm{y},n+1} = \sigma_{\mathrm{y}}(X_{0,n+1}) = \sigma_{\mathrm{y},0}(X_{0,n+1})^q \tag{55}$$

which is easily obtained combining (14) and (20).

The solution algorithm steps (1)–(3) are graphically represented in Figure 1(b).

Remark 4.1
The relative stress and backstress can be calculated whenever needed as

$$\boldsymbol{\Sigma} = \frac{\mathbf{X}^s}{X_0}\sigma_{\mathrm{y}} \tag{56}$$

$$\boldsymbol{\alpha} = H_{\mathrm{kin}}\frac{2G\mathbf{e} - \boldsymbol{\Sigma}}{2G + H_{\mathrm{kin}}} \tag{57}$$

The first one is immediately obtained from the definition of $\mathbf{X}$, while the second one follows from (4) and (5), observing that $\boldsymbol{\alpha} = H_{\mathrm{kin}}\mathbf{e}^{\mathrm{p}}$.

Remark 4.2
The variable X_0 is a local auxiliary variable and not an history variable. In other words, introducing an appropriate scaling of the vector $\mathbf{X}$ the variable X_0 does not need to be updated at every time step. See Remark 3 in Reference [2] for a deeper explanation of these algorithmical issues.

Remark 4.3
Whenever $H_{\mathrm{iso}} = 0$, i.e. there is no isotropic hardening, the solution obtained with this scheme is exact. Other exact integrators can be found in the literature for the case $H_{\mathrm{iso}} = 0$, see for example References [13–15]. A discussion of exponential-based exact integration schemes and other exact integrators can be found in Reference [2].

4.3. Tangent matrix

The algorithmically consistent tangent matrix can be obtained properly linearizing the time-discrete procedure. In the present paragraph all the dynamical discrete quantities are evaluated at the end of the actual time step t_{n+1}; therefore all subscripts will be omitted for the sake of compactness.

For the total stress, Equation (5) provides

$$\frac{\partial \mathbf{s}}{\partial \mathbf{e}} = \frac{\partial \boldsymbol{\Sigma}}{\partial \mathbf{e}} + \frac{\partial \boldsymbol{\alpha}}{\partial \mathbf{e}} \tag{58}$$

and, recalling also Equation (57), it becomes

$$\frac{\partial \mathbf{s}}{\partial \mathbf{e}} = \frac{2G}{2G + H_{\text{kin}}} \frac{\partial \boldsymbol{\Sigma}}{\partial \mathbf{e}} + \frac{2G H_{\text{kin}}}{2G + H_{\text{kin}}} \mathbb{I} \tag{59}$$

We also have

$$\frac{\partial \mathbf{s}}{\partial \boldsymbol{\varepsilon}} = \frac{\partial \mathbf{s}}{\partial \mathbf{e}} \frac{\partial \mathbf{e}}{\partial \boldsymbol{\varepsilon}} = \frac{\partial \mathbf{s}}{\partial \mathbf{e}} \mathbb{I}_{\text{dev}} \tag{60}$$

where

$$\mathbb{I}_{\text{dev}} = \mathbb{I} - \tfrac{1}{3}(\mathbf{i}\mathbf{i}^{\text{T}}) \tag{61}$$

Taking into account the volumetric part of the stress, from Equations (1)–(3) we obtain the tangent matrix

$$\mathbb{D}_{\text{disc}} = \frac{\partial \boldsymbol{\sigma}}{\partial \boldsymbol{\varepsilon}} = \frac{\partial \mathbf{s}}{\partial \boldsymbol{\varepsilon}} + K(\mathbf{i}\mathbf{i}^{\text{T}}) \tag{62}$$

Joining statements (59), (60) and (62) we obtain

$$\mathbb{D}_{\text{disc}} = \frac{\partial \boldsymbol{\sigma}}{\partial \boldsymbol{\varepsilon}} = \frac{2G}{2G + H_{\text{kin}}} \frac{\partial \boldsymbol{\Sigma}}{\partial \mathbf{e}} \mathbb{I}_{\text{dev}} + \frac{2G H_{\text{kin}}}{2G + H_{\text{kin}}} \mathbb{I}_{\text{dev}} + K(\mathbf{i}\mathbf{i}^{\text{T}}) \tag{63}$$

From the definition of the *generalized stress vector* $\mathbf{X}$ we get

$$\frac{\partial \mathbf{X}^{\text{s}}}{\partial \mathbf{e}} = \frac{X_0}{\sigma_{\text{y}}} \frac{\partial \boldsymbol{\Sigma}}{\partial \mathbf{e}} + \frac{\boldsymbol{\Sigma}}{\sigma_{\text{y}}} \frac{\partial X_0}{\partial \mathbf{e}} + X_0 \boldsymbol{\Sigma} \frac{\partial}{\partial \mathbf{e}} \left(\frac{1}{\sigma_{\text{y}}} \right) \tag{64}$$

Recalling (55), a direct derivation gives

$$\frac{\partial}{\partial \mathbf{e}} \left(\frac{1}{\sigma_{\text{y}}} \right) = \frac{1}{\sigma_{\text{y},0}} \frac{\partial}{\partial \mathbf{e}} X_0^{-q} = -q \frac{1}{X_0 \sigma_{\text{y}}} \frac{\partial X_0}{\partial \mathbf{e}} \tag{65}$$

From (64) and (65), using also definition (23) it is easy to derive

$$\frac{\partial \boldsymbol{\Sigma}}{\partial \mathbf{e}} = \frac{\sigma_{\text{y}}}{X_0} \left(\frac{\partial \mathbf{X}^{\text{s}}}{\partial \mathbf{e}} - \frac{1 - q}{X_0} \mathbf{X}^{\text{s}} \frac{\partial X_0}{\partial \mathbf{e}} \right) \tag{66}$$

For the elastic phase we immediately have

$$\frac{\partial \mathbf{X}^{\text{s}}}{\partial \mathbf{e}} = 2G X_0 \mathbb{I} \tag{67}$$

$$\frac{\partial X_0}{\partial \mathbf{e}} = \mathbf{0} \tag{68}$$

while in the plastic phase the result is far more complicated and it can be found in Appendix A.

5. THEORETICAL ANALYSIS OF ALGORITHMICAL PROPERTIES

In this section we address from a theoretical point of view the following algorithmical properties for the ESC and ESC^2 methods: yield consistency, exactness under proportional loading, accuracy and convergence. In particular we will prove that the ESC scheme is yield consistent and converging with linear rate to the exact solution. The ESC^2 scheme is yield consistent, exact in the case of proportional loading and quadratically accurate. Moreover, limiting the proof to purely plastic load histories, we show that the ESC^2 scheme is quadratically convergent. Although purely plastic loadings are not uncommon in practical cases, a more complete approach should deal with generic loading histories; hence, this point is worth further investigation.

Finally, both schemes are exact in the case of materials with no isotropic hardening. Note that the word 'exact' means that the algorithm introduces no error for strain driven load histories under the classical hypothesis $\dot{\mathbf{e}}$ piecewise constant. In practical applications this does not translate directly into exactness of the constitutive solver. This point will be cleared by the numerical tests and it will be briefly discussed in Section 6.4.

For basic results and definitions regarding the numerical integration of ordinary differential equations we refer for example to References [16, 17].

5.1. Yield consistency

In the framework of the new formulation, recalling (17) and (23), the yield consistency condition

$$\|\boldsymbol{\Sigma}_{n+1}\| = \sigma_{\mathrm{y},n+1} \quad \text{at end of each plastic step} \tag{69}$$

becomes

$$\|\mathbf{X}^{\mathrm{s}}_{n+1}\|^2 - X^2_{0,n+1} = 0 \quad \text{at end of each plastic step} \tag{70}$$

Both the ESC and ESC^2 schemes are yield consistent, in other words satisfy condition (70). The proof for the ESC^2 is identical to the one for the ESC method, which is shown in Reference [2].

5.2. Exactness whenever $H_{\mathrm{iso}} = 0$

Both the ESC and ESC^2 schemes are exact whenever there is no isotropic hardening. The proof of this property is immediate, considering that in such cases the matrices (30)–(31) are constant in each time step. For other methods with this property see mainly References [13, 14].

5.3. Exactness under proportional loading

Assume as usual a piecewise linear strain history. We then say that a particular algorithmical time step develops under proportional loading if during the whole step

$$\boldsymbol{\Sigma}(t) = r(t)\boldsymbol{\Sigma}_0 \tag{71}$$

where $\boldsymbol{\Sigma}_0$ is the initial stress and $r(t)$ is a scalar depending on time. It is easy to check that the definition above implies

$$\dot{\mathbf{e}} = \|\dot{\mathbf{e}}\| \frac{\boldsymbol{\Sigma}_0}{\|\boldsymbol{\Sigma}_0\|} = \|\dot{\mathbf{e}}\| \frac{\boldsymbol{\Sigma}}{\|\boldsymbol{\Sigma}\|} \tag{72}$$

during the time step. As noted in Reference [2], the radial return map algorithm is exact in the case of proportional loading, while this same property in not shared by the ESC scheme. This means that, if a given time step develops under proportional loading, then the solution obtained with the return map will be identical to the continuous solution with the same initial step conditions. As shown in the following proposition, differently form the ESC scheme, the ESC^2 method has the advantage of being exact in the case of proportional loading.

We have the following.

Proposition 5.1
The ESC^2 algorithm is exact in the case of proportional loading.

Proof
It is trivial to show that the scheme is exact during the elastic part of each time step; therefore what has to be proved is that the algorithm is exact also in the plastic part of each step. In the case of purely plastic steps ($\alpha = 0$) this follows from Lemma 5.1 below, while the general case ($\alpha > 0$) follows applying a trivial modification of the same lemma. □

In the sequel, we will call the *direction* of a vector $\mathbf{v} \in \mathbb{R}^n$ the normalized unit vector $\mathbf{v}/\|\mathbf{v}\|$.

Lemma 5.1
Consider a purely plastic step under proportional loading. Then the solution obtained with the ESC^2 is identical to the continuous solution with the same initial step conditions.

Proof
As usual we mark with the subindex n the values at the start of the step, which are assumed assigned. Note that, being the step purely plastic, the initial relative stress $\boldsymbol{\Sigma}_n$ lays on the yield surface. As already noted, the proportional loading assumption implies that during the step

$$\dot{\mathbf{e}} = \|\dot{\mathbf{e}}\| \frac{\boldsymbol{\Sigma}_n}{\|\boldsymbol{\Sigma}_n\|} \tag{73}$$

or equivalently

$$\Delta\mathbf{e} = \|\Delta\mathbf{e}\| \frac{\boldsymbol{\Sigma}_n}{\|\boldsymbol{\Sigma}_n\|} \tag{74}$$

In the case of proportional loading the continuous solution can be checked to be equal to

$$\boldsymbol{\Sigma}^{\mathrm{ex}}_{n+1} = \frac{\boldsymbol{\Sigma}_n}{\|\boldsymbol{\Sigma}_n\|} \sigma^{\mathrm{ex}}_{\mathrm{y},n+1} \tag{75}$$

$$\sigma^{\mathrm{ex}}_{\mathrm{y},n+1} = \sigma_{\mathrm{y},n} + 2Gq\|\Delta\mathbf{e}\| \tag{76}$$

where here and in the sequel the index e is used to indicate the exact solution.

The value of the backstress $\boldsymbol{\alpha}$ at any instant can be immediately derived from the value of $\boldsymbol{\Sigma}$ and relation (57); this is true both for the continuous and the numerical solution. Similarly, the remaining variables can then be obtained from the usual relations (3)–(10). Therefore all that has to be checked in order to state the Lemma is that the value $\boldsymbol{\Sigma}_{n+1}$ obtained with the ESC^2 algorithm is equal to $\boldsymbol{\Sigma}^{\mathrm{ex}}_{n+1}$.

This will be done in two steps. The first is to prove that the direction of $\boldsymbol{\Sigma}_{n+1}$ is the same as the one of $\boldsymbol{\Sigma}^{\mathrm{ex}}_{n+1}$, in other words that the direction of $\boldsymbol{\Sigma}_{n+1}$ is equal to $\boldsymbol{\Sigma}_n/\|\boldsymbol{\Sigma}_n\|$. The second step is to show that the norm of $\boldsymbol{\Sigma}_{n+1}$ is the same as the one of $\boldsymbol{\Sigma}^{\mathrm{ex}}_{n+1}$, in other words that the norm of $\boldsymbol{\Sigma}_{n+1}$ is equal to $\sigma^{\mathrm{ex}}_{\mathrm{y},n+1}$.

Step 1: By definition of $\mathbf{X}^{\mathrm{s}}_n$ and recalling that $\|\boldsymbol{\Sigma}_n\| = \sigma_{\mathrm{y},n}$ we have

$$\mathbf{X}^{\mathrm{s}}_n = X_{0,n}\frac{\boldsymbol{\Sigma}_n}{\|\boldsymbol{\Sigma}_n\|} \tag{77}$$

Applying the algorithm (see (44) and (54)), we get

$$\mathbf{X}^{\mathrm{s}}_{n+1} = \mathbf{X}^{\mathrm{s}}_n + \left(\left[\frac{(a-1)}{\|\Delta\mathbf{e}\|^2}\right]\Delta\mathbf{e}\cdot\mathbf{X}^{\mathrm{s}}_n + \frac{bX_{0,n}}{\|\Delta\mathbf{e}\|}\right)\Delta\mathbf{e} \tag{78}$$

where

$$a = \cosh\left(\frac{2G}{R}\|\Delta\mathbf{e}\|\right) \tag{79}$$

$$b = \sinh\left(\frac{2G}{R}\|\Delta\mathbf{e}\|\right) \tag{80}$$

with R defined in (40). Joining (78) with (74) and (77) immediately gives that $\mathbf{X}^{\mathrm{s}}_{n+1}$ is of the form

$$\mathbf{X}^{\mathrm{s}}_{n+1} = \psi\frac{\boldsymbol{\Sigma}_n}{\|\boldsymbol{\Sigma}_n\|} \quad \psi\in\mathbb{R} \tag{81}$$

which immediately implies

$$\frac{\mathbf{X}^{\mathrm{s}}_{n+1}}{\|\mathbf{X}^{\mathrm{s}}_{n+1}\|} = \frac{\boldsymbol{\Sigma}_n}{\|\boldsymbol{\Sigma}_n\|} \tag{82}$$

First from definitions (17) and (23), then from (82) and finally using (75), we obtain

$$\frac{\boldsymbol{\Sigma}_{n+1}}{\|\boldsymbol{\Sigma}_{n+1}\|} = \frac{\mathbf{X}^{\mathrm{s}}_{n+1}}{\|\mathbf{X}^{\mathrm{s}}_{n+1}\|} = \frac{\boldsymbol{\Sigma}_n}{\|\boldsymbol{\Sigma}_n\|} = \frac{\boldsymbol{\Sigma}^{\mathrm{ex}}_{n+1}}{\|\boldsymbol{\Sigma}^{\mathrm{ex}}_{n+1}\|} \tag{83}$$

This completes the first part of the proof.

Step 2: Being the step plastic and due to the consistency of the scheme, we have

$$\|\boldsymbol{\Sigma}_{n+1}\| = \sigma_{\mathrm{y},n+1} \tag{84}$$

which, recalling relation (55) and with simple algebra, gives

$$\|\boldsymbol{\Sigma}_{n+1}\| = \sigma_{\mathrm{y},n+1} = \sigma_{\mathrm{y},0}(X_{0,n+1})^q = \sigma_{\mathrm{y},0}(X_{0,n})^q\left(\frac{X_{0,n+1}}{X_{0,n}}\right)^q = \sigma_{\mathrm{y},n}\left(\frac{X_{0,n+1}}{X_{0,n}}\right)^q \tag{85}$$

Again applying the algorithm (see (44) and (54)), we get

$$X_{0,n+1} = b\frac{\Delta\mathbf{e}\cdot\mathbf{X}_n^{\mathrm{s}}}{\|\Delta\mathbf{e}\|} + aX_{0,n} \tag{86}$$

Substituting (74) and (77) in (86) and dividing by $X_{0,n}$ gives immediately

$$\frac{X_{0,n+1}}{X_{0,n}} = b\|\Delta\mathbf{e}\|\frac{\dfrac{\boldsymbol{\Sigma}_n}{\|\boldsymbol{\Sigma}_n\|}\cdot\dfrac{\boldsymbol{\Sigma}_n}{\|\boldsymbol{\Sigma}_n\|}}{\|\Delta\mathbf{e}\|} + a = b + a \tag{87}$$

which by definition of a and b gives

$$\frac{X_{0,n+1}}{X_{0,n}} = \exp\left(\frac{2G}{R}\|\Delta\mathbf{e}\|\right) \tag{88}$$

Substituting (88) into (85) we obtain

$$\|\boldsymbol{\Sigma}_{n+1}\| = \sigma_{\mathrm{y},n}\exp\left(\frac{2Gq}{R}\|\Delta\mathbf{e}\|\right) \tag{89}$$

Due to (75), (76) and (89), in order to show that

$$\|\boldsymbol{\Sigma}_{n+1}\| = \|\boldsymbol{\Sigma}_{n+1}^{\mathrm{ex}}\| \tag{90}$$

and conclude the proof of the lemma, it suffices to show that

$$\sigma_{\mathrm{y},n}\exp\left(\frac{2Gq}{R}\|\Delta\mathbf{e}\|\right) = \sigma_{\mathrm{y},n} + 2Gq\|\Delta\mathbf{e}\| \tag{91}$$

Identity (91) follows from a direct calculation and the definition of R in (40), observing that from (74) and (77)

$$c = \frac{2Gq\|\Delta\mathbf{e}\|}{\sigma_{\mathrm{y},n}} \tag{92}$$

□

5.4. Accuracy

In this section we analyse the accuracy of the methods ESC and ESC^2.

It is easy to check that the function $R(\Delta t)$, defined in (40), is continuous even in $\Delta t = 0$. Moreover, it holds the following result which will be useful in the sequel.

Lemma 5.2

Let $\alpha = 0$ (purely plastic step). Then the (right) derivative in $\Delta t = 0$ of the function $R(\Delta t)$ defined in (40) is well defined and equal to

$$\dot{R}(0) = \frac{\dot{\sigma}_{\mathrm{y}}(t_n)}{2} \tag{93}$$

Moreover, it exists the second (right) derivative in zero of $R(\Delta t)$.

Applying the definition of derivative and (40) we obtain

$$\dot{R}(0) = \lim_{\Delta t \to 0} \frac{R(\Delta t) - R(0)}{\Delta t} = \sigma_{y,n} \lim_{\Delta t \to 0} \frac{c - \ln(1+c)}{\ln(1+c)\Delta t}$$

$$= \sigma_{y,n} \lim_{\Delta t \to 0} \frac{c^2/2}{c\Delta t} = \frac{2Gq}{2} \frac{\mathbf{X}_n^s}{X_{0,n}} \cdot \dot{\mathbf{e}} \tag{94}$$

where we also used the condition $\alpha = 0$. Due to definition (23), identity (94) gives

$$\dot{R}(0) = \frac{2Gq}{2} \frac{\boldsymbol{\Sigma}_n}{\|\boldsymbol{\Sigma}_n\|} \cdot \dot{\mathbf{e}} \tag{95}$$

Recalling that we are in plastic phase, a direct derivation gives

$$\dot{\sigma}_y = \frac{d}{dt} \|\boldsymbol{\Sigma}\| = \frac{\boldsymbol{\Sigma}}{\|\boldsymbol{\Sigma}\|} \cdot \dot{\boldsymbol{\Sigma}} \tag{96}$$

Starting from the von-Mises constitutive equations, in Section 4 of Reference [1] it is shown that in plastic phases

$$\dot{\boldsymbol{\Sigma}} + (2G + H_{kin}) \frac{\boldsymbol{\Sigma}}{\sigma_{y,0} + H_{iso}\gamma} \dot{\gamma} = 2G\dot{\mathbf{e}} \tag{97}$$

$$(\sigma_{y,0} + H_{iso}\gamma)(2G + H_{kin} + H_{iso})\dot{\gamma} = 2G\dot{\mathbf{e}} \cdot \boldsymbol{\Sigma} \tag{98}$$

Extracting the expression for $\dot{\gamma}$ in (98) and using it in (97), we immediately obtain an equation for $\dot{\boldsymbol{\Sigma}}$; then, taking the scalar product with $\boldsymbol{\Sigma}/\|\boldsymbol{\Sigma}\|$ we get

$$\dot{\boldsymbol{\Sigma}} \cdot \frac{\boldsymbol{\Sigma}}{\|\boldsymbol{\Sigma}\|} = 2G\dot{\mathbf{e}} \cdot \frac{\boldsymbol{\Sigma}}{\|\boldsymbol{\Sigma}\|} - \frac{(2G + H_{kin})\boldsymbol{\Sigma} \cdot \boldsymbol{\Sigma}}{\|\boldsymbol{\Sigma}\|(\sigma_{y,0} + H_{iso}\gamma)} \frac{2G\dot{\mathbf{e}} \cdot \boldsymbol{\Sigma}}{(\sigma_{y,0} + H_{iso}\gamma)(2G + H_{kin} + H_{iso})} \tag{99}$$

Recalling that $\sigma_{y,0} + \gamma H_{iso} = \|\boldsymbol{\Sigma}\|$, Equation (99) immediately simplifies to

$$\dot{\boldsymbol{\Sigma}} \cdot \frac{\boldsymbol{\Sigma}}{\|\boldsymbol{\Sigma}\|} = 2Gq\dot{\mathbf{e}} \cdot \frac{\boldsymbol{\Sigma}}{\|\boldsymbol{\Sigma}\|} \tag{100}$$

Equations (96) and (100) give at time t_n

$$\dot{\sigma}_y(t_n) = 2Gq\dot{\mathbf{e}} \cdot \frac{\boldsymbol{\Sigma}_n}{\|\boldsymbol{\Sigma}_n\|} \tag{101}$$

which joined with (95) proves (93).

Finally, the last statement of the lemma can be derived from the definition of second-order derivative

$$\ddot{R}(0) = \lim_{\Delta t \to 0^+} \frac{\dot{R}(\Delta t) - \dot{R}(0)}{\Delta t} \tag{102}$$

calculating the value of $\dot{R}(\Delta t)$ directly from (40), using (95) for the value of $\dot{R}(0)$ and then calculating the limit in (102). □

We are now ready to present the following accuracy result.

Proposition 5.2
The ESC^2 scheme holds quadratic accuracy, in other words the truncation error is of order $(\Delta t)^2$ with Δt size of the time step. The ESC scheme holds instead linear accuracy.

Proof
We will show the proof only in the case of the ESC^2 method; the proof for the ESC scheme is simpler and follows similar steps. As usual, it is sufficient to show that the truncation error for the relative stress $\mathbf{\Sigma}$ is quadratic; the result for the back stress $\boldsymbol{\alpha}$ follows from relation (57). Therefore, assuming all the variables at time t_n as given, we want to show that

$$T_n = \frac{\|\mathbf{\Sigma}^{\text{ex}}_{n+1} - \mathbf{\Sigma}_{n+1}\|}{\Delta t} = O(\Delta t^2) \tag{103}$$

where $\mathbf{\Sigma}^{\text{ex}}_{n+1}$ is the exact solution for the given initial data at time t_{n+1} and $\mathbf{\Sigma}_{n+1}$ the solution obtained with the ESC^2 scheme for the same initial data at time t_{n+1}.

We will start showing that

$$\|\mathbf{X}^{\text{ex}}_{n+1} - \mathbf{X}_{n+1}\| = O(\Delta t^3) \tag{104}$$

where again $\mathbf{X}^{\text{ex}}_{n+1}$ represents the exact generalized stress for the given initial data at time t_{n+1} and $\mathbf{X}_{n+1}$ the solution obtained with the ESC^2 algorithm for the same initial data.

Recalling that the scheme is exact during elastic phases, it is sufficient to prove the proposition for purely plastic steps. The result for mixed elasto-plastic steps will then follow trivially considering the plastic part of the step as a purely plastic step with smaller Δt. We assume therefore a purely plastic step (i.e. $\alpha = 0$) with given initial data at time t_n.

Then, from (11), the exact value of the *generalized stress*

$$\mathbf{X}^{\text{ex}}_{n+1} = \mathbf{X}^{\text{ex}}(t_{n+1}) = \mathbf{X}^{\text{ex}}(t_n + \Delta t) \tag{105}$$

is the solution at time $t_n + \Delta t$ of the dynamical system

$$\begin{aligned} &\mathbf{X}^{\text{ex}}(t_n) = \mathbf{X}_n \\ &\dot{\mathbf{X}}^{\text{ex}}(t) = \frac{2G}{\sigma_y}\mathbb{B}\,\mathbf{X}^{\text{ex}}(t) \quad t \in [t_n, t_n + \Delta t] \end{aligned} \tag{106}$$

where the matrix

$$\mathbb{B} = \begin{pmatrix} 0_{6\times 6} & \dot{\mathbf{e}} \\ \dot{\mathbf{e}}^{\text{T}} & 0 \end{pmatrix} \tag{107}$$

and where we recall that σ_y may vary in time. Following instead the scheme ESC^2, the value of the *generalized stresses*

$$\mathbf{X}_{n+1} = \mathbf{X}(t_{n+1}) = \mathbf{X}(t_n + \Delta t) \tag{108}$$

is

$$\mathbf{X}(t_n + \Delta t) = \exp\left(\frac{2G}{R}\mathbb{B}\,\Delta t\right)\mathbf{X}_n \tag{109}$$

where $R = R(\Delta t)$ depends on Δt as shown in (40).

It can be checked after some calculation that both $\mathbf{X}^{\text{ex}}(t_n+\Delta t)$ and $\mathbf{X}(t_n+\Delta t)$ are C^3 regular as functions of Δt, even in $\Delta t = 0$. Therefore, a truncated Taylor expansion immediately leads to

$$\mathbf{X}^{\text{ex}}(t_n + \Delta t) = \mathbf{X}^{\text{ex}}(t_n) + \frac{\mathrm{d}\mathbf{X}^{\text{ex}}}{\mathrm{d}\Delta t}(t_n)\Delta t + \frac{\mathrm{d}^2\mathbf{X}^{\text{ex}}}{\mathrm{d}\Delta t^2}(t_n)\frac{\Delta t^2}{2} + O(\Delta t^3) \tag{110}$$

$$\mathbf{X}(t_n + \Delta t) = \mathbf{X}(t_n) + \frac{\mathrm{d}\mathbf{X}}{\mathrm{d}\Delta t}(t_n)\Delta t + \frac{\mathrm{d}^2\mathbf{X}}{\mathrm{d}\Delta t^2}(t_n)\frac{\Delta t^2}{2} + O(\Delta t^3) \tag{111}$$

As a consequence, in order to prove (104), we must show that

$$\mathbf{X}^{\text{ex}}(t_n) = \mathbf{X}(t_n) \tag{112}$$

$$\frac{\mathrm{d}\mathbf{X}^{\text{ex}}}{\mathrm{d}\Delta t}(t_n) = \frac{\mathrm{d}\mathbf{X}}{\mathrm{d}\Delta t}(t_n) \tag{113}$$

$$\frac{\mathrm{d}^2\mathbf{X}^{\text{ex}}}{\mathrm{d}\Delta t^2}(t_n) = \frac{\mathrm{d}^2\mathbf{X}}{\mathrm{d}\Delta t^2}(t_n) \tag{114}$$

Using (106) and with direct derivations we easily obtain for the exact solution

$$\mathbf{X}^{\text{ex}}(t_n) = \mathbf{X}_n \tag{115}$$

$$\frac{\mathrm{d}\mathbf{X}^{\text{ex}}}{\mathrm{d}\Delta t}(t_n) = \dot{\mathbf{X}}^{\text{ex}}(t_n) = \frac{2G}{\sigma_{\text{y},n}}\mathbb{B}\,\mathbf{X}^{\text{ex}}(t_n) = \frac{2G}{\sigma_{\text{y},n}}\mathbb{B}\,\mathbf{X}_n \tag{116}$$

$$\begin{aligned}\frac{\mathrm{d}^2\mathbf{X}^{\text{ex}}}{\mathrm{d}\Delta t^2}(t_n) = \ddot{\mathbf{X}}^{\text{ex}}(t_n) &= \frac{2G}{\sigma_{\text{y},n}}\mathbb{B}\,\dot{\mathbf{X}}^{\text{ex}}(t_n) - \frac{2G}{\sigma^2_{\text{y},n}}\mathbb{B}\,\mathbf{X}^{\text{ex}}(t_n)\dot{\sigma}_{\text{y}}(t_n)\\ &= \left(\frac{2G}{\sigma_{\text{y},n}}\mathbb{B}\right)^2\mathbf{X}_n - \frac{2G}{\sigma^2_{\text{y},n}}\mathbb{B}\,\mathbf{X}_n\dot{\sigma}_{\text{y}}(t_n)\end{aligned} \tag{117}$$

For the discrete solution, from (109) we immediately have

$$\mathbf{X}(t_n) = \mathbf{X}_n \tag{118}$$

which joined with (115) gives (112).

First again from (109) and then a direct derivation lead to

$$\begin{aligned}\frac{\mathrm{d}\mathbf{X}}{\mathrm{d}\Delta t}(t_n) &= \left[\frac{\mathrm{d}}{\mathrm{d}\Delta t}\exp\left(\frac{2G}{R(\Delta t)}\mathbb{B}\,\Delta t\right)\right]_{\Delta t=0}\mathbf{X}_n \\ &= \left[\frac{2G}{R(\Delta t)}\mathbb{B} - \frac{2G}{R(\Delta t)^2}\mathbb{B}\,\Delta t\,\dot{R}(\Delta t)\right]_{\Delta t=0}\left[\exp\left(\frac{2G}{R(\Delta t)}\mathbb{B}\,\Delta t\right)\right]_{\Delta t=0}\mathbf{X}_n \\ &= \frac{2G}{R(0)}\mathbb{B}\,\mathbf{X}_n = \frac{2G}{\sigma_{\mathrm{y},n}}\mathbb{B}\,\mathbf{X}_n \end{aligned} \tag{119}$$

where we implicitly used that $\dot{R}(0)$ is well defined due to Lemma 5.2.

Identity (119) joined with (116) gives (113). Deriving (119) we obtain

$$\begin{aligned}\frac{\mathrm{d}^2\mathbf{X}}{\mathrm{d}\Delta t^2}(t_n) &= \left\{\frac{\mathrm{d}}{\mathrm{d}\Delta t}\left[\frac{2G}{R(\Delta t)}\mathbb{B} - \frac{2G}{R(\Delta t)^2}\mathbb{B}\,\Delta t\,\dot{R}(\Delta t)\right]\left[\exp\left(\frac{2G}{R(\Delta t)}\mathbb{B}\,\Delta t\right)\right]\right\}_{\Delta t=0}\mathbf{X}_n \\ &= \left\{\left[\frac{2G}{R(\Delta t)}\mathbb{B} - \frac{2G}{R(\Delta t)^2}\mathbb{B}\,\Delta t\,\dot{R}(\Delta t)\right]^2 - 2\frac{2G}{R(\Delta t)^2}\mathbb{B}\dot{R}(\Delta t) + 2\frac{2G}{R(\Delta t)^3}\mathbb{B}\,\Delta t\,\dot{R}(\Delta t)^2\right. \\ &\quad \left. - \frac{2G}{R(\Delta t)^2}\mathbb{B}\Delta t\,\ddot{R}(\Delta t)\right\}_{\Delta t=0}\left[\exp\left(\frac{2G}{R(\Delta t)}\mathbb{B}\,\Delta t\right)\right]_{\Delta t=0}\mathbf{X}_n \\ &= \left[\left(\frac{2G}{\sigma_{\mathrm{y},n}}\mathbb{B}\right)^2 - 2\frac{2G}{\sigma_{\mathrm{y},n}^2}\mathbb{B}\,\dot{R}(0)\right]\mathbf{X}_n \end{aligned} \tag{120}$$

where we implicitly used that $\ddot{R}(0)$ is well defined due to Lemma 5.2.

Identity (114) then follows from (117), (120) and again Lemma 5.2. We have proven the three identities (112)–(114), therefore the proof of (104) follows as already discussed. First from definitions (17) and (23), then using relation (55) it follows the relation between relative and *generalized stress*

$$\boldsymbol{\Sigma} = \sigma_{\mathrm{y}}\frac{\mathbf{X}^{\mathrm{s}}}{X_0} = \sigma_{\mathrm{y},0}X_0^{q-1}\mathbf{X}^{\mathrm{s}} \tag{121}$$

Using (121) and (104) and without showing all the calculations we finally get

$$\|\boldsymbol{\Sigma}_{n+1}^{\mathrm{ex}} - \boldsymbol{\Sigma}_{n+1}\| = \|\sigma_{\mathrm{y},0}(X_{0,n+1}^{\mathrm{ex}})^{q-1}\mathbf{X}_{n+1}^{\mathrm{s,e}} - \sigma_{\mathrm{y},0}(X_{0,n+1})^{q-1}\mathbf{X}_{n+1}^{\mathrm{s}}\| = O(\Delta t^3) \tag{122}$$

Bound (122) immediately implies (103) and proves the proposition. □

5.5. Convergence

In this section we will make a first study of the convergence properties of the ESC and ESC^2 methods. In order to keep calculations simpler we will address the case with no kinematic hardening (i.e. $H_{\mathrm{kin}} = 0$), otherwise also the norm introduced below should be modified

accordingly. Note that this is not restrictive because, differently from isotropic hardening, an opportune translation in stress space shows that linear kinematic hardening does not generate additional difficulties from the numerical viewpoint.

We will consider convergence in the classical 'complementary Helmholtz free energy' norm

$$|||\boldsymbol{\Sigma}, \sigma_{\mathrm{y}}|||^2 = (2G)^{-1}\|\boldsymbol{\Sigma}\|^2 + (H_{\mathrm{iso}})^{-1}\sigma_{\mathrm{y}}^2 \tag{123}$$

Note that, although on a finite dimensional space all norms are equivalent, the choice of this norm is not arbitrary. This is in fact the norm in which the original continuous problem is contractive; see for example References [3, 18]. Note also that we are assuming $H_{\mathrm{iso}}>0$, otherwise both schemes are exact and there is nothing to prove.

Given a certain degree of accuracy, probably the best way to prove the convergence of a scheme in plasticity is to show that the scheme is B-stable, in other words that the method is contractive in the 'complementary Helmholtz free energy' norm above (see Reference [6]). On the other hand, the aim of this section is not to address strong properties as the B-Stability (see References [6, 18]) which, considering the particular formulation under consideration, would require a deeper study. We will therefore prove convergence directly, essentially by showing that in the energy norm the error propagates at a controlled rate. In other words

- For the ESC scheme we prove linear convergence.
- For the ESC^2 scheme we show quadratic convergence, but only for purely plastic load histories. On one hand, considering that during elastic phases there is virtually no additional error, an assumption of this kind, which is also addressed in the classical paper [6], can be reasonably accepted. On the other hand, in the presence of complicated histories with a large number of elastic-plastic switches, a result of this kind is not sufficient to guarantee convergence; the matter is surely worth further investigations.

In order to fix the notation, we note that in the sequel we will refer to the general stress–radius couples $(\boldsymbol{\Sigma}, \sigma_{\mathrm{y}})$ simply as 'couples'. The convergence of the methods will derive from the accuracy results of the previous chapter and from the two following propositions, which state the stable behaviour of the error propagation in the scheme.

Proposition 5.3

Assume that two initial couples $(\boldsymbol{\Sigma}_i, \sigma_{\mathrm{y},i})$ and $(\tilde{\boldsymbol{\Sigma}}_i, \tilde{\sigma}_{\mathrm{y},i})$ and a strain increment $\Delta\mathbf{e}$ are assigned. Let $(\boldsymbol{\Sigma}_f, \sigma_{\mathrm{y},f})$ and $(\tilde{\boldsymbol{\Sigma}}_f, \tilde{\sigma}_{\mathrm{y},f})$ be the solutions obtained applying one step of the ESC algorithm with strain increment $\Delta\mathbf{e}$, respectively, to $(\boldsymbol{\Sigma}_i, \sigma_{\mathrm{y},i})$ and $(\tilde{\boldsymbol{\Sigma}}_i, \tilde{\sigma}_{\mathrm{y},i})$. Then there exists a constant K such that

$$|||\boldsymbol{\Sigma}_f - \tilde{\boldsymbol{\Sigma}}_f, \sigma_{\mathrm{y},f} - \tilde{\sigma}_{\mathrm{y},f}||| \leqslant \exp(K\|\Delta\mathbf{e}\|)|||\boldsymbol{\Sigma}_i - \tilde{\boldsymbol{\Sigma}}_i, \sigma_{\mathrm{y},i} - \tilde{\sigma}_{\mathrm{y},i}||| \tag{124}$$

Moreover, the constant K depends only on $\|\Delta\mathbf{e}\|$ and is bounded on all sets of the type $\{\Delta\mathbf{e} \in \mathbb{R}^6,\ \ \|\Delta\mathbf{e}\| \leqslant c,\ \ c \in \mathbb{R}^+\}$.

Proof

In order to shorten the notation, during the proof an added index E will in general refer to the difference

$$\boldsymbol{\Sigma}^E = \boldsymbol{\Sigma} - \tilde{\boldsymbol{\Sigma}}, \quad \sigma_{\mathrm{y}}^E = \sigma_{\mathrm{y}} - \tilde{\sigma}_{\mathrm{y}} \tag{125}$$

The proof can be divided into three separate cases, depending on which type of step (elastic or plastic) each of the two couples is following. It is not restrictive to assume that each couple is undergoing either a totally plastic or a totally elastic step; it is then trivial to check that the proof for mixed elasto-plastic increments simply follows splitting the time step opportunely.

If both couples follow an elastic step, then both couples undergo the same identical transformation and the proposition is trivially true setting $K = 0$. If both couples are in plastic phase, or if one is in plastic and the other in elastic phase, the matter is more complicated. In both cases, Lemmas A.1 and A.2 (see Appendix A), respectively, show that the error will evolve satisfying the bound

$$\frac{\mathrm{d}}{\mathrm{d}t}|||\boldsymbol{\Sigma}^E(t), \sigma_{\mathrm{y}}^E(t)||| \leqslant \|\dot{\mathbf{e}}\|[K_1|||\boldsymbol{\Sigma}^E(t_0), \sigma_y^E(t_0)||| + K_2|||\boldsymbol{\Sigma}^E(t), \sigma_y^E(t)|||] \tag{126}$$

during the whole time step. In the present case, respectively, at the beginning and at the end of an integration interval, it holds

$$(\boldsymbol{\Sigma}(t_0), \sigma_{\mathrm{y}}(t_0)) = (\boldsymbol{\Sigma}_i, \sigma_{\mathrm{y},i}) \quad (\boldsymbol{\Sigma}_f, \sigma_{\mathrm{y},f}) = (\boldsymbol{\Sigma}(t_0 + \Delta t), \sigma_{\mathrm{y}}(t_0 + \Delta t)) \tag{127}$$

$$(\tilde{\boldsymbol{\Sigma}}(t_0), \tilde{\sigma}_{\mathrm{y}}(t_0)) = (\tilde{\boldsymbol{\Sigma}}_i, \tilde{\sigma}_{\mathrm{y},i}) \quad (\tilde{\boldsymbol{\Sigma}}_f, \tilde{\sigma}_{\mathrm{y},f}) = (\tilde{\boldsymbol{\Sigma}}(t_0 + \Delta t), \tilde{\sigma}_{\mathrm{y}}(t_0 + \Delta t)) \tag{128}$$

$$(\boldsymbol{\Sigma}^E(t_0), \sigma_{\mathrm{y}}^E(t_0)) = (\boldsymbol{\Sigma}_i^E, \sigma_{\mathrm{y},i}^E) \quad (\boldsymbol{\Sigma}_f^E, \sigma_{\mathrm{y},f}^E) = (\boldsymbol{\Sigma}^E(t_0 + \Delta t), \sigma_{\mathrm{y}}^E(t_0 + \Delta t)) \tag{129}$$

assuming that the time-step has length Δt. We now have, for all $t \in [t_0, t_0 + \Delta t]$

$$|||\boldsymbol{\Sigma}^E(t), \sigma_{\mathrm{y}}^E(t)||| = |||\boldsymbol{\Sigma}^E(t_0), \sigma_{\mathrm{y}}^E(t_0)||| + \int_{t_0}^{t_0+t} \frac{\mathrm{d}}{\mathrm{d}s}|||\boldsymbol{\Sigma}^E(s), \sigma_y^E(s)||| \,\mathrm{d}s \tag{130}$$

Applying bound (126) in Equation (130) now easily gives

$$\begin{aligned} |||\boldsymbol{\Sigma}^E(t), \sigma_{\mathrm{y}}^E(t)||| &\leqslant [1 + K_1\|\dot{\mathbf{e}}\|(t - t_0)]|||\boldsymbol{\Sigma}^E(t_0), \sigma_{\mathrm{y}}^E(t_0)||| \\ &\quad + \|\dot{\mathbf{e}}\|K_2 \int_{t_0}^{t_0+t} |||\boldsymbol{\Sigma}^E(s), \sigma_y^E(s)||| \,\mathrm{d}s \quad \forall t \in [t_0, t_0 + \Delta t] \end{aligned} \tag{131}$$

which in turn, recalling that $t \in [t_0, t_0 + \Delta t]$, grants

$$\begin{aligned} |||\boldsymbol{\Sigma}^E(t), \sigma_{\mathrm{y}}^E(t)||| &\leqslant [1 + K_1\|\dot{\mathbf{e}}\|\Delta t]|||\boldsymbol{\Sigma}^E(t_0), \sigma_{\mathrm{y}}^E(t_0)||| \\ &\quad + \|\dot{\mathbf{e}}\|K_2 \int_{t_0}^{t_0+t} |||\boldsymbol{\Sigma}^E(s), \sigma_y^E(s)||| \,\mathrm{d}s \quad \forall t \in [t_0, t_0 + \Delta t] \end{aligned} \tag{132}$$

A scalar function which satisfies a condition of this type must, due to the Gronwall Lemma (see for example References [16, 17]), satisfy on the same interval the bound

$$|||\boldsymbol{\Sigma}^E(t), \sigma_{\mathrm{y}}^E(t)||| \leqslant [1 + K_1\|\dot{\mathbf{e}}\|\Delta t]|||\boldsymbol{\Sigma}^E(t_0), \sigma_{\mathrm{y}}^E(t_0)||| \exp[K_2\|\dot{\mathbf{e}}\|(t - t_0)] \tag{133}$$

Using bound (133) for $t = t_0 + \Delta t$ and observing that $1 + x \leqslant \exp(x)$ for all $x \in \mathbb{R}$, it follows

$$|||\boldsymbol{\Sigma}_f^E, \sigma_{y,f}^E||| \leqslant \exp[K_1 \|\dot{\mathbf{e}}\| \Delta t] |||\boldsymbol{\Sigma}_i^E, \sigma_{y,i}^E||| \exp[K_2 \|\dot{\mathbf{e}}\| \Delta t] \tag{134}$$

where we also used the definitions (128) and (129). Finally, recalling that $\|\Delta \mathbf{e}\| = \|\dot{\mathbf{e}}\| \Delta t$ and setting $K = K_1 + K_2$, bound (134) gives

$$|||\boldsymbol{\Sigma}_f^E, \sigma_{y,f}^E||| \leqslant \exp[K \|\Delta \mathbf{e}\|] |||\boldsymbol{\Sigma}_i^E, \sigma_{y,i}^E||| \tag{135}$$

The proposition is proved. □

The proof of the following result is identical to the previous one, the only difference being to limit the argument to plastic steps, therefore using only Lemma A.1 instead of Lemma A.2 (see Appendix A).

Proposition 5.4
Assume that two initial couples $(\boldsymbol{\Sigma}_i, \sigma_{y,i})$ and $(\tilde{\boldsymbol{\Sigma}}_i, \tilde{\sigma}_{y,i})$ and a strain increment $\Delta \mathbf{e}$ are assigned. Let $(\boldsymbol{\Sigma}_f, \sigma_{y,f})$ and $(\tilde{\boldsymbol{\Sigma}}_f, \tilde{\sigma}_{y,f})$ be the solutions obtained applying one purely plastic step of the ESC^2 algorithm with strain increment $\Delta \mathbf{e}$, respectively, to $(\boldsymbol{\Sigma}_i, \sigma_{y,i})$ and $(\tilde{\boldsymbol{\Sigma}}_i, \tilde{\sigma}_{y,i})$. Then there exists a constant K such that

$$|||\boldsymbol{\Sigma}_f - \tilde{\boldsymbol{\Sigma}}_f, \sigma_{y,f} - \tilde{\sigma}_{y,f}||| \leqslant \exp(K \|\Delta \mathbf{e}\|) |||\boldsymbol{\Sigma}_i - \tilde{\boldsymbol{\Sigma}}_i, \sigma_{y,i} - \tilde{\sigma}_{y,i}||| \tag{136}$$

Moreover, the constant K depends only on $\|\Delta \mathbf{e}\|$ and is bounded on all sets of the type $\{\Delta \mathbf{e} \in \mathbb{R}^6, \ \|\Delta \mathbf{e}\| \leqslant c, \ c \in \mathbb{R}^+\}$.

Remark 5.1
Note that the second part of Lemma A.2 in the Appendix, i.e. proving that the scalar A_2 in the lemma is non-positive, can be proved identically also for the ESC^2 scheme. The additional difficulty is instead given by bounding the scalar A_1 with terms which depend only on the present or past history. Note that following the same steps a conditional stability result could be obtained for the ESC^2 scheme in case of mixed elasto-plastic evolution histories (i.e. a result as in Proposition 5.3 with the additional assumption that $\Delta \mathbf{e}$ is sufficiently small).

We can now state the convergence result for the ESC^2 method, which holds for purely plastic load histories. This is undoubtedly a non-negligible limitation, as noted in the comments at the start of this section. The matter is therefore worth further investigation.

Proposition 5.5
Let a piecewise linear strain history $\mathbf{e}(t)$, $t \in [0, T]$ and two starting couples $(\boldsymbol{\Sigma}^{ex}(0), \sigma_y^{ex}(0))$ and $(\boldsymbol{\Sigma}(0), \sigma_y(0))$ be assigned. Assume for simplicity that $\|\dot{\mathbf{e}}\|$ is constant during the whole history; due to the rate invariance of the problem, this is not restrictive. Let the time interval be divided into N uniform sub-intervals of length $\Delta t = T/N$. Let $(\boldsymbol{\Sigma}^{ex}(T), \sigma_y^{ex}(T))$ indicate the exact solution at time T following the strain history above with starting point $(\boldsymbol{\Sigma}^{ex}(0), \sigma_y^{ex}(0))$; let also $(\boldsymbol{\Sigma}(T), \sigma_y(T))$ indicate the solution at time T obtained with the ESC^2 scheme based on the above strain history and time stepping, with starting point $(\boldsymbol{\Sigma}(0), \sigma_y(0))$. Finally, assume that the strain history is such that the continuous and the discrete solutions undergo

a purely plastic loading. Then

$$|||(\boldsymbol{\Sigma}^{\mathrm{ex}}(T), \sigma_{\mathrm{y}}^{\mathrm{ex}}(T)) - (\boldsymbol{\Sigma}(T), \sigma_{\mathrm{y}}(T))|||$$

$$\leqslant C_1 \|\dot{\mathbf{e}}\|^2 (\Delta t)^2 + C_2 |||(\boldsymbol{\Sigma}^{\mathrm{ex}}(0), \sigma_{\mathrm{y}}^{\mathrm{ex}}(0)) - (\boldsymbol{\Sigma}(0), \sigma_{\mathrm{y}}(0))||| \tag{137}$$

where C_1, C_2 are independent of N.

Proof

In the sequel a subindex n will indicate a variable calculated at time $t_n = n\Delta t$, $n = \{0, 1, 2, \ldots, N\}$. Given any stress–radius couple $(\tilde{\boldsymbol{\Sigma}}, \tilde{\sigma}_{\mathrm{y}})$, let in the sequel $\Theta_n[\tilde{\boldsymbol{\Sigma}}, \tilde{\sigma}_{\mathrm{y}}]$ indicate the couple obtained applying one step of the ESC^2 scheme to $(\tilde{\boldsymbol{\Sigma}}, \tilde{\sigma}_{\mathrm{y}})$ with $\Delta\mathbf{e} = \mathbf{e}_{n+1} - \mathbf{e}_n = \mathbf{e}(t_{n+1}) - \mathbf{e}(t_n)$. We have in particular for the discrete solution

$$(\boldsymbol{\Sigma}, \sigma_{\mathrm{y}})_{n+1} = \Theta_n[\boldsymbol{\Sigma}_n, \sigma_{\mathrm{y},n}] \tag{138}$$

Using the definition of the operator Θ and a triangle inequality, for the error at time t_{n+1} it holds

$$E_{n+1} := |||(\boldsymbol{\Sigma}^{\mathrm{ex}}, \sigma_{\mathrm{y}}^{\mathrm{ex}})_{n+1} - (\boldsymbol{\Sigma}, \sigma_{\mathrm{y}})_{n+1}|||$$

$$\leqslant |||(\boldsymbol{\Sigma}^{\mathrm{ex}}, \sigma_{\mathrm{y}}^{\mathrm{ex}})_{n+1} - \Theta_n[\boldsymbol{\Sigma}_n^{\mathrm{ex}}, \sigma_{\mathrm{y},n}^{\mathrm{ex}}]||| + |||\Theta_n[\boldsymbol{\Sigma}_n^{\mathrm{ex}}, \sigma_{\mathrm{y},n}^{\mathrm{ex}}] - \Theta_n[\boldsymbol{\Sigma}_n, \sigma_{\mathrm{y},n}]||| \tag{139}$$

The first member in the right-hand side of (139) represents the local error generated at each time step, which can be controlled using the accuracy results of the previous section. The second member represents instead the propagation of the accumulated error, which must be dealt with essentially using the stability results of this section.

From Proposition 5.2 and bound (104), recalling that $\sigma_{\mathrm{y}} = \sigma_{\mathrm{y},0} X_0^q$ both for the exact and the numerical solution, it follows

$$|||(\boldsymbol{\Sigma}^{\mathrm{ex}}, \sigma_{\mathrm{y}}^{\mathrm{ex}})_{n+1} - \Theta_n[\boldsymbol{\Sigma}_n^{\mathrm{ex}}, \sigma_{\mathrm{y},n}^{\mathrm{ex}}]||| \leqslant \tilde{C}(\Delta t)^3 \tag{140}$$

where here and in the sequel $\tilde{C}$ will indicate a general constant independent of N. We want to rewrite bound (140) in rate invariant form. The error in Proposition 5.2 follows from the difference between the third-order derivative of the numerical scheme and the exact solution. Therefore, it is easy to check that, bringing out the dependence of $\tilde{C}$ on $\|\dot{\mathbf{e}}\|$, bound (141) becomes

$$|||(\boldsymbol{\Sigma}^{\mathrm{ex}}, \sigma_{\mathrm{y}}^{\mathrm{ex}})_{n+1} - \Theta_n[\boldsymbol{\Sigma}_n^{\mathrm{ex}}, \sigma_{\mathrm{y},n}^{\mathrm{ex}}]||| \leqslant \tilde{C}\|\dot{\mathbf{e}}\|^3 (\Delta t)^3 = \tilde{C}\|\Delta\mathbf{e}\|^3 \tag{141}$$

where the new constant $\tilde{C}$ is now rate invariant. For the second member in the right-hand side of (139), Proposition 5.4 gives

$$|||\Theta_n[\boldsymbol{\Sigma}_n^{\mathrm{ex}}, \sigma_{\mathrm{y},n}^{\mathrm{ex}}] - \Theta_n[\boldsymbol{\Sigma}_n, \sigma_{\mathrm{y},n}]||| \leqslant \exp(K\|\Delta\mathbf{e}\|)|||(\boldsymbol{\Sigma}_n^{\mathrm{ex}}, \sigma_{\mathrm{y},n}^{\mathrm{ex}}) - (\boldsymbol{\Sigma}_n, \sigma_{\mathrm{y},n})|||$$

$$= \exp(K\|\Delta\mathbf{e}\|) E_n \tag{142}$$

with K fixed scalar independent of N. Therefore, applying the bounds (141) and (142) into the inequality (139), we get

$$E_{n+1} \leqslant \tilde{C}\|\Delta\mathbf{e}\|^3 + \exp(K\|\Delta\mathbf{e}\|)E_n \tag{143}$$

Iteration of (143) easily leads to

$$E_N \leqslant \tilde{C}\|\Delta\mathbf{e}\|^3 \left[\sum_{n=0}^{N-1} \exp(Kn\|\Delta\mathbf{e}\|)\right] + \exp(KN\|\Delta\mathbf{e}\|)E_0 \tag{144}$$

From (144), using that $\Delta\mathbf{e} = \dot{\mathbf{e}}\Delta t$ and $T = N\Delta t$ we get

$$\begin{aligned} E_N &\leqslant \tilde{C}\|\Delta\mathbf{e}\|^3 N \exp(KN\|\Delta\mathbf{e}\|) + \exp(KN\|\Delta\mathbf{e}\|)E_0 \\ &\leqslant \tilde{C}(\|\dot{\mathbf{e}}\|^2(\Delta t)^2\|\dot{\mathbf{e}}\|T + E_0)\exp(K\|\dot{\mathbf{e}}\|T) \leqslant \tilde{C}'(\|\dot{\mathbf{e}}\|^2(\Delta t)^2 + E_0) \end{aligned} \tag{145}$$

where the scalar $\tilde{C}'$ is rate invariant and independent of N. Note that also the quantities $\|\dot{\mathbf{e}}\|^2(\Delta t)^2$ and $\|\dot{\mathbf{e}}\|T$ appearing in (145) are correctly rate invariant. Recalling the definition of E_n, $n \in \{0, 1, 2, \ldots, N\}$, the proposition is proved. □

Remark 5.2
The convergence result for the ESC method is not restricted to purely plastic load histories. The result is identical to that of Proposition 5.5 but holding for any type of loading history. The proof is essentially the same as for Proposition 5.5 but using the more general Proposition 5.3 instead of Proposition 5.4.

6. NUMERICAL TESTS

In this section we present a set of numerical examples which enable a detailed comparison of all the previously considered methods. For the sake of compactness we systematically adopt the following acronyms:

- *RM*: Backward Euler return map method [3–5];
- *MPT*: Midpoint return map method [6];
- *ENN*: Exponential Non-symmetric Non-consistent method [1];
- *ENC*: Exponential Non-symmetric Consistent method [2, 10];
- *ESC*: Exponential Symmetric Consistent method (Section 3, [2, 10]);
- *ESC*^{2}: Exponential Symmetric Consistent 2nd-order accurate method (Section 3).

The numerical tests are divided in three parts. To investigate the algorithm accuracy and precision, we consider piecewise stress–strain load histories with different time discretizations and plot the respective error graphs (Section 6.1). To explore the algorithm precision in particular when using large time steps we present iso-error maps for the RM, MPT and ESC^2 algorithms (Section 6.2). To test the algorithm performance in terms of Newton iteration convergence, we consider two boundary value problems regarding the elongation of rectangular perforated strips in a plane strain regime (Section 6.3). The piecewise numerical tests and the iso-error maps are performed with the aid of the CE-Driver [19], while the boundary value problems

are solved using the finite element code FEAP [20]. In the analysis we adopt three distinct sets of material constants:

- Material 1 (see Reference [21])

$$E = 100\,\text{MPa}, \qquad \nu = 0.3$$
$$\sigma_{\text{y},0} = 15\,\text{MPa}, \qquad H_{\text{kin}} = 10\,\text{MPa}, \qquad H_{\text{iso}} = 10\,\text{MPa}$$
$$\bar{\sigma}_{y,0} = \sigma_{\text{y},0}/E = 0.15, \quad \bar{H}_{\text{kin}} = H_{\text{kin}}/E = 0.1, \quad \bar{H}_{\text{iso}} = H_{\text{iso}}/E = 0.1$$

- Material 2 (see Reference [3])

$$E = 30\,000\,\text{MPa}, \qquad \nu = 0.3$$
$$\sigma_{\text{y},0} = 3\,\text{MPa}, \qquad H_{\text{kin}} = 0\,\text{MPa}, \qquad H_{\text{iso}} = 0\,\text{MPa}$$
$$\bar{\sigma}_{y,0} = \sigma_{\text{y},0}/E = 0.0001, \quad \bar{H}_{\text{kin}} = H_{\text{kin}}/E = 0, \quad \bar{H}_{\text{iso}} = H_{\text{iso}}/E = 0$$

- Material 3 (see Reference [5])

$$E = 7000\,\text{MPa}, \qquad \nu = 0.3,$$
$$\sigma_{\text{y},0} = 24.3\,\text{MPa}, \qquad H_{\text{kin}} = 0\,\text{MPa}, \qquad H_{\text{iso}} = 225\,\text{MPa}$$
$$\bar{\sigma}_{y,0} = \sigma_{\text{y},0}/E = 0.0034, \quad \bar{H}_{\text{kin}} = H_{\text{kin}}/E = 0, \quad \bar{H}_{\text{iso}} = H_{\text{iso}}/E = 0.032$$

Finally, we recall that the Young's modulus E and the Poisson ratio ν uniquely determine the constants K and G as follows:

$$K = \frac{E}{3(1-2\nu)}, \quad G = \frac{E}{2(1+\nu)}$$

Remark 6.1
Clearly, at the computational level, the limit equation (48) on the trial solution is checked numerically. We assume the trial state to be on the yield surface whenever the absolute value of the difference between the r.h.s. and the l.h.s. is lower than a tolerance fixed on 10^{-12} throughout the numerical tests presented in this section.

6.1. Pointwise stress--strain tests

We consider three biaxial non-proportional stress–strain histories obtained assuming to control two strain components and four stress components, respectively, i.e.

Problem 1: ε_{11} σ_{22} σ_{33} ε_{12} σ_{13} σ_{23}

Problem 2: ε_{11} ε_{22} σ_{33} σ_{12} σ_{13} σ_{23}

Problem 3: ε_{11} σ_{22} σ_{33} ε_{12} σ_{13} σ_{23}

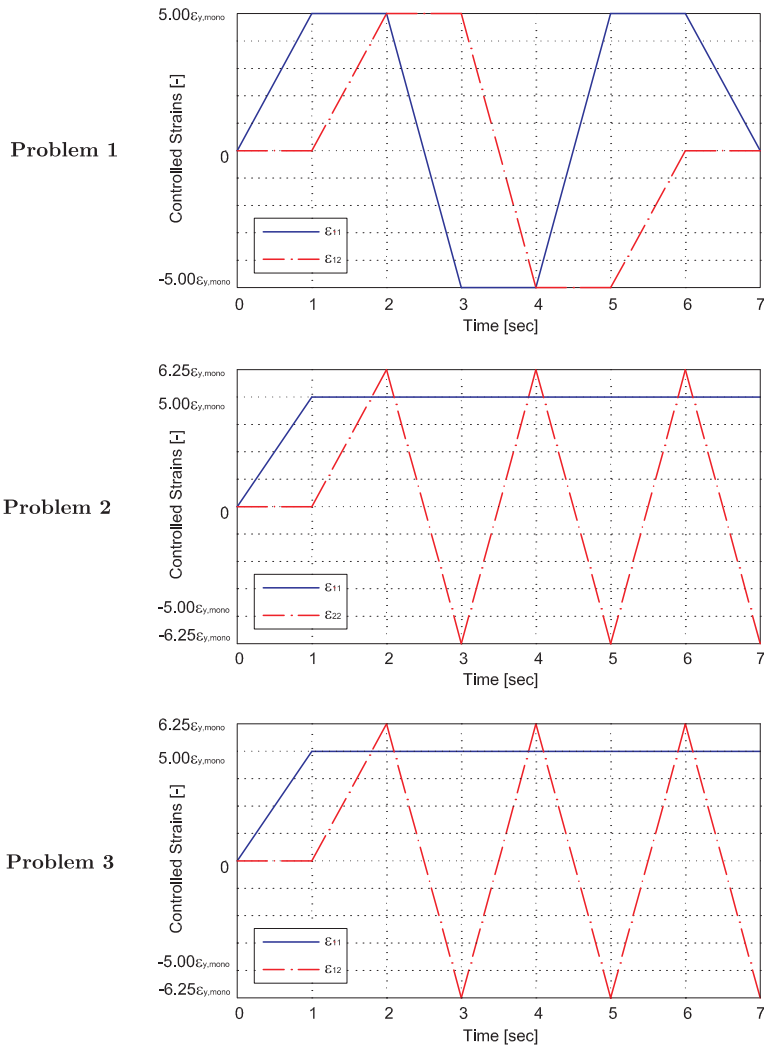

Figure 2. Pointwise stress–strain tests. Mixed stress–strain load histories for Problems 1–3.

For each history we require that all the controlled stress components are identically equal to zero, while the strains are varied proportionally to

$$\varepsilon_{\mathrm{y,mono}} = \sqrt{\frac{3}{2}}\frac{\sigma_{\mathrm{y},0}}{E} \tag{146}$$

which represents the first yielding strain value in a uniaxial loading history. A graphical representation of the varying quantities is given in Figure 2.

Lacking the analytical solutions of the problems under investigation, we compute the 'exact' solutions using the midpoint scheme with a very fine time discretization, corresponding to 100 000 steps per second ($\Delta t = 0.00001$ s). Such 'exact' solutions are compared with the

'numerical' ones, corresponding, respectively, to 10, 20 and 40 steps per second ($\Delta t = 0.1, 0.05, 0.025$ s) and computed with the quadratic algorithms MPT, ENC and ESC^2, respectively.

The error is evaluated separately for the stress and the strain introducing the following relative norms:

$$E_n^{\boldsymbol{\sigma}} = \frac{\|\boldsymbol{\sigma}_n - \boldsymbol{\sigma}_n^{\mathrm{ex}}\|}{\sigma_{\mathrm{y},n}}, \quad E_n^{\boldsymbol{\varepsilon}} = 2G\frac{\|\boldsymbol{\varepsilon}_n - \boldsymbol{\varepsilon}_n^{\mathrm{ex}}\|}{\sigma_{\mathrm{y},n}} \tag{147}$$

where $\|\bullet\|$ indicates the usual Euclidean vector norm and $\sigma_{\mathrm{y},n}$ is the yield surface radius at time t_n. In Equations (147), $\boldsymbol{\sigma}_n$ and $\boldsymbol{\varepsilon}_n$ as well as $\boldsymbol{\sigma}_n^{\mathrm{ex}}$ and $\boldsymbol{\varepsilon}_n^{\mathrm{ex}}$ are, respectively, the stress–strain 'numerical' and 'exact' solution at time t_n. The error measure (147) is chosen due to the high variation of the problem solution, which makes inappropriate the use of the classical relative error:

$$\hat{E}_n^{\boldsymbol{\sigma}} = \frac{\|\boldsymbol{\sigma}_n - \boldsymbol{\sigma}_n^{\mathrm{ex}}\|}{\|\boldsymbol{\sigma}_n^{\mathrm{ex}}\|}, \quad \hat{E}_n^{\boldsymbol{\varepsilon}} = 2G\frac{\|\boldsymbol{\varepsilon}_n - \boldsymbol{\varepsilon}_n^{\mathrm{ex}}\|}{\|\boldsymbol{\varepsilon}_n^{\mathrm{ex}}\|} \tag{148}$$

Figure 3 reports stress and strain relative errors (147) using Material 1 for the first load history and for the three different time discretizations indicated above; Figure 4 repeats the process for Material 3. It is evident from the error plots that

- The performance of the MPT and the ENC methods are comparable. The MPT algorithm provides exact solutions for the case of proportional loading. Finally, as the step size is reduced, both methods converge quadratically, i.e. the error is divided by 4 every time the number of steps is doubled (the error goes as Δt^2).
- The new symmetric method ESC^2 grants relatively lower error levels than the MPT and ESC algorithms for all the considered stress–strain histories. Also in this case, the numerical solution is exact for proportional loading conditions and the error decreases quadratically with respect to the time step size.

We omit, for brevity's sake, to provide the error plots regarding the remaining load histories since they would lead to conclusions similar to those given in the above points.

In order to further investigate the rate of convergence of the method, we also introduce the *total error* as the ℓ^1 norm in time of the absolute error

$$E_T^{\boldsymbol{\sigma}} = \sum_{n=1}^{N} \Delta t\, E_n^{\boldsymbol{\sigma}}, \quad E_T^{\boldsymbol{\varepsilon}} = \sum_{n=1}^{N} \Delta t\, E_n^{\boldsymbol{\varepsilon}} \tag{149}$$

Then, in Figure 5 we plot the total error versus the number of time steps in logarithmic scale for the six methods RM, MPT, ENN, ENC, ESC and ESC^2 for Problem 1 with Material 1. The quadratic convergence of the MPT, ENC, ENN and ESC^2 methods with respect to the linear convergence of the other algorithms can be clearly appreciated. It is remarkable that even this error measurement qualifies the new optimal ESC^2 scheme as the most precise within the set of the tested algorithms.

6.2. Iso-error maps

Iso-error maps are commonly adopted in the literature (see for example References [3, 6, 13, 22]) as a systematic tool to test the accuracy of plasticity integration algorithms. Error maps are plotted as a result of particular piecewise mixed stress–strain loading histories.

Each loading history is set up by controlling the ε_{11} and ε_{22} strain components and keeping the remaining stresses equal to zero. The evolution in time of the controlled quantities is

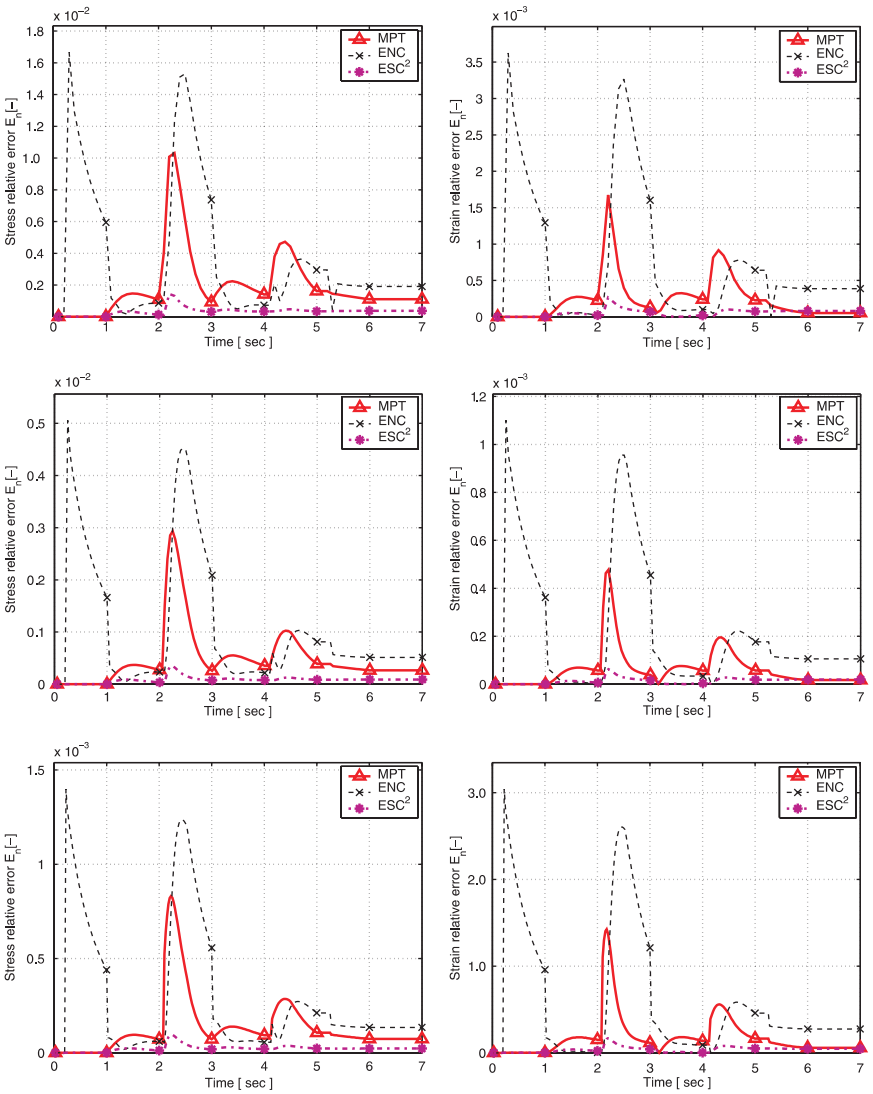

Figure 3. Pointwise stress–strain tests: Problem 1 with Material 1. Stress and strain error for $\Delta t = 0.1,\ 0.05$ and 0.025 s.

piecewise linear and can be divided in two distinct phases defined as follows (see Table I). Phase 1 consists of a purely elastic path and proceeds from the zero stress and strain state (State 0) to a specific state on the yield surface (State 1) given in terms of the yield strain components $\varepsilon_{11,y}$ and $\varepsilon_{22,y}$. Phase 2 is a purely plastic path which starts from State 1 and leads to a final state (State 2) given in terms of the strain increments $\Delta\varepsilon_{11}$ and $\Delta\varepsilon_{22}$.

In this analysis, we consider three different choices of State 1, corresponding to plane states of stress on the yield surface [3], labelled **A**, **B** and **C**, respectively, represented in Figure 6 and

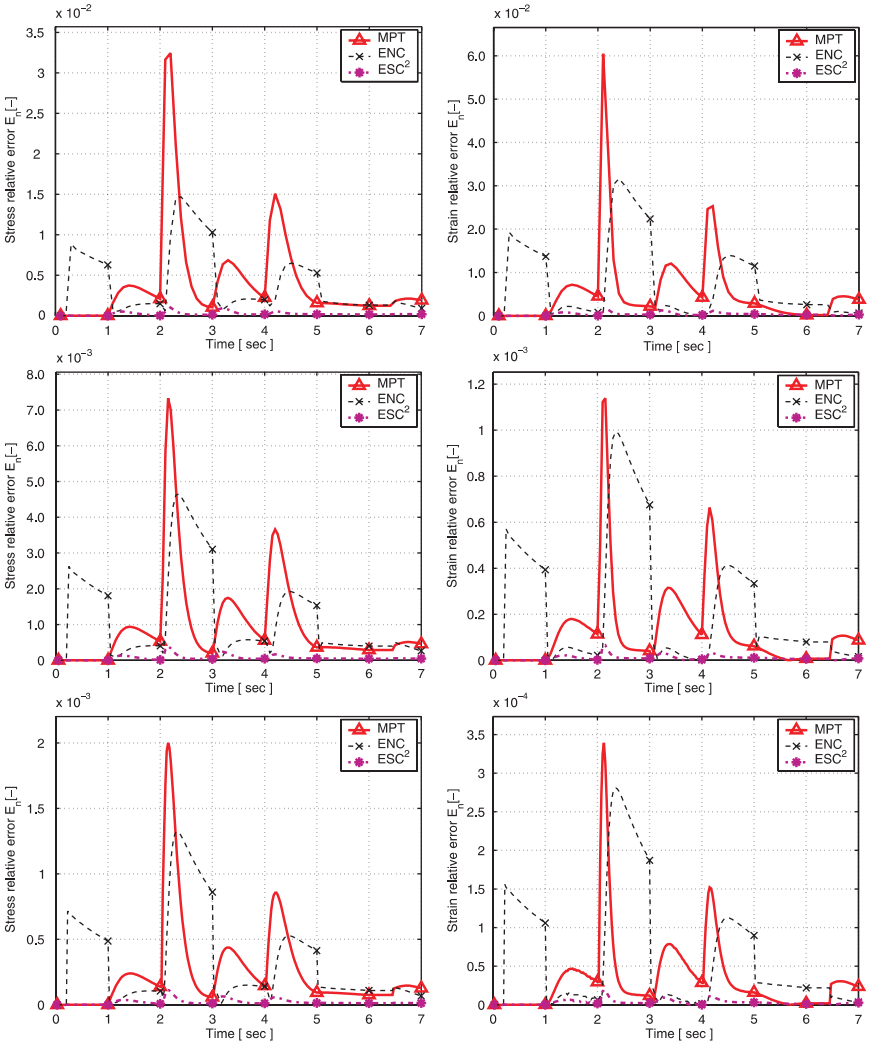

Figure 4. Pointwise stress–strain tests: Problem 1 with Material 3. Stress and strain error for $\Delta t = 0.1,\ 0.05$ and 0.025 s.

corresponding to uniaxial, biaxial and pure shear states. Each State 1 is expressed in Table II in terms of the quantity $\varepsilon_{y,\mathrm{mono}}$ (uniaxial yield strain) already defined in (146).

We solve a total of 60×60 mixed stress–strain histories for each State 1, corresponding to the following sets of normalized strain increments (see Figures 7–9):

$$\frac{\Delta\varepsilon_{11}}{\varepsilon_{11,y}} = 0, 0.1, 0.2, \ldots, 6$$

$$\frac{\Delta\varepsilon_{22}}{\varepsilon_{22,y}} = 0, 0.1, 0.2, \ldots, 6$$

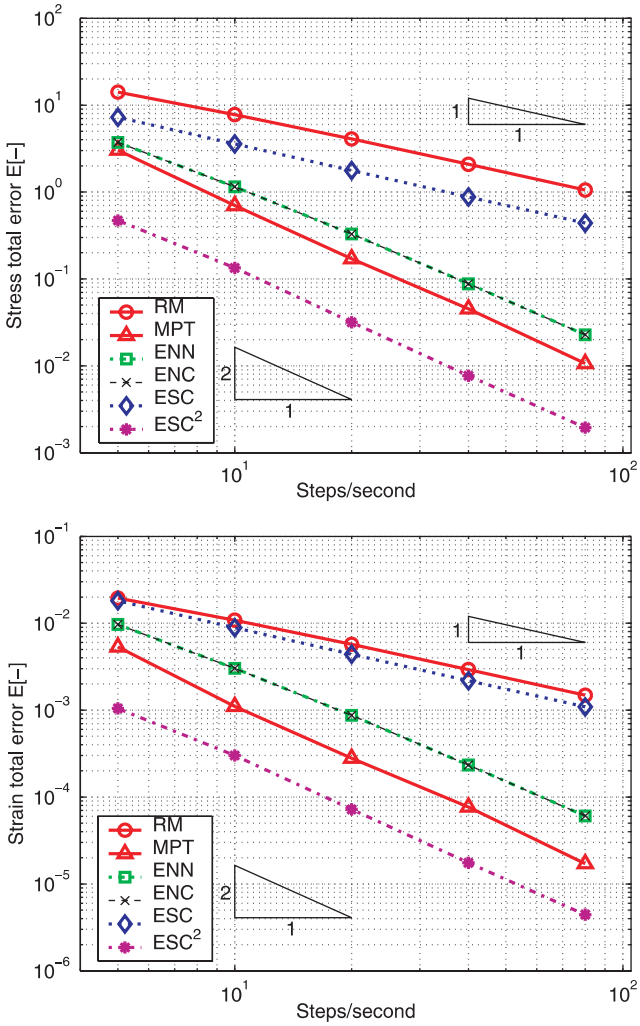

Figure 5. Pointwise stress–strain tests. Problem 1 with Material 1. Stress and strain total error *versus* number of steps per second.

Table I. Benchmark mixed stress–strain history for iso-error maps computation.

	Time (s)	ε_{11}	ε_{22}	σ_{33}	σ_{12}	σ_{13}	σ_{23}
State 0	$t=0$	0	0	0	0	0	0
State 1	$t=1$	$\varepsilon_{11,y}$	$\varepsilon_{22,y}$	0	0	0	0
State 2	$t=2$	$\varepsilon_{y,11}+\Delta\varepsilon_{11}$	$\varepsilon_{y,22}+\Delta\varepsilon_{22}$	0	0	0	0

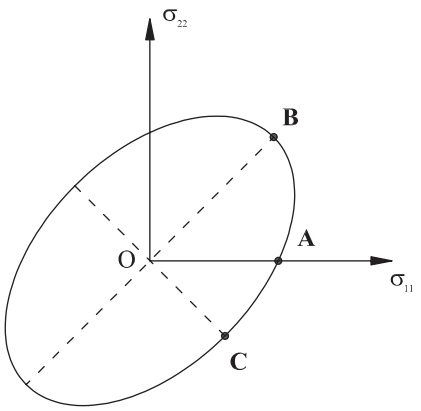

Figure 6. Plane stress von-Mises yield surface representation in principal stresses plane. State 1 choices for iso-error maps plots.

Table II. Iso-error maps. Choices for the State 1 point on the yield surface.

State 1	$\varepsilon_{11,y}$	$\varepsilon_{22,y}$	σ_{33}	σ_{12}	σ_{13}	σ_{23}
A	$\varepsilon_{y,\text{mono}}$	$-\nu\varepsilon_{y,\text{mono}}$	0	0	0	0
B	$(1-\nu)\varepsilon_{y,\text{mono}}$	$\varepsilon_{y,\text{mono}}$	0	0	0	0
C	$\frac{(1+\nu)}{3}\varepsilon_{y,\text{mono}}$	$-\frac{(1+\nu)}{3}\varepsilon_{y,\text{mono}}$	0	0	0	0

This subdivision leads to a total of 3600 computed mixed stress–strain histories and to an equal number of calculated error percentage values, according to the following expression:

$$E_{\text{iso}}^{\sigma} = \frac{\|\boldsymbol{\sigma} - \boldsymbol{\sigma}^{\text{ex}}\|}{\|\boldsymbol{\sigma}^{\text{ex}}\|} \tag{150}$$

where $\boldsymbol{\sigma}$ is the final stress tensor, computed adopting a single time step discretization whereas $\boldsymbol{\sigma}^{\text{ex}}$ corresponds to an 'exact' solution obtained with a very fine time step. All the calculations refer to Material 2 [3].

The total error range is subdivided in ten equally spaced levels according to which the iso-curves are drawn in Figures 7–9. Each iso-curve is indicated by a proper error label while the thick continuous line represents the zero-level error stress–strain histories (i.e. proportional loading histories). For the sake of completeness, aside from each map we also report the maximum error value computed on the grid adopted for the computation of the iso-error map.

Observing Figures 7–9, we recognize that the ESC^2 scheme produces more precise solutions in terms of stresses if compared to the RM and MPT algorithms. Even for 'large' strain increments the new exponential-based procedure reveals low levels of error compared with the other two methods. Such a result seems to be rather interesting since it suggests robustness of the integration scheme for practical application of the integration procedure in a finite element analysis of boundary value problems. It is also worth noting that the RM scheme, which has

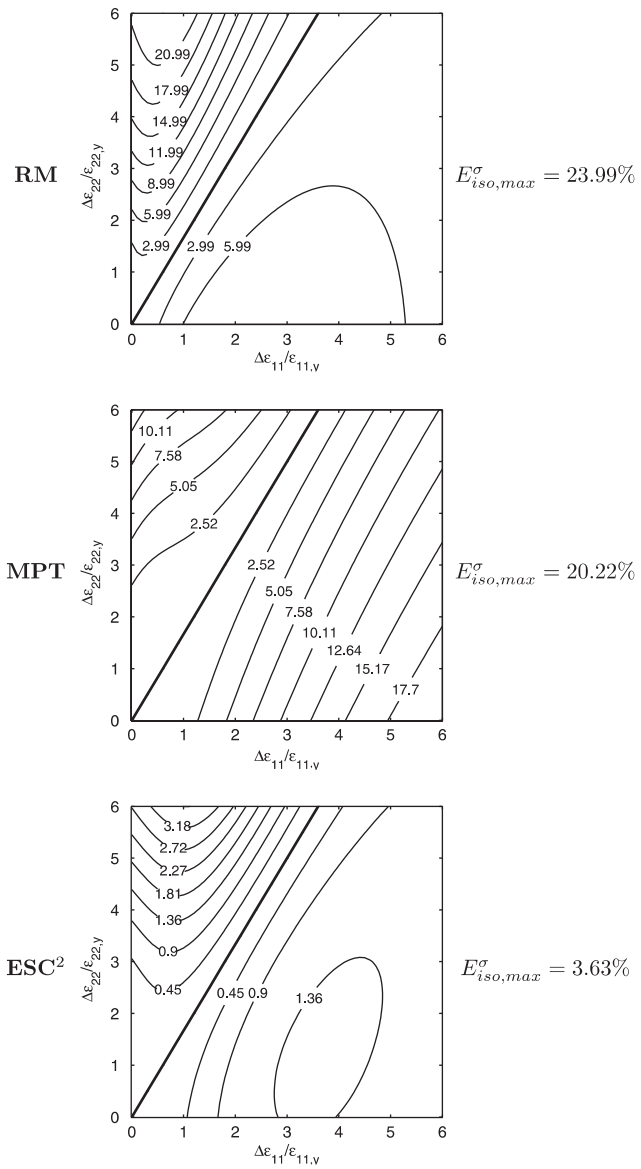

Figure 7. Comparison between return map (RM), midpoint (MPT) and the new exponential-based scheme (ESC^2). Iso-error maps for yield surface State 1—A and indication of the maximum stress error level.

linear accuracy, is more precise than the quadratic MPT algorithm for large strain increments. In this sense the ESC^2 method turns out to be the most reliable within the three methods, since it is quadratic and maintains good behaviour also for large time steps.

A further observation is that, although $H_{\text{iso}} = 0$, the exponential-based algorithm presents a non-zero error. This apparently erroneous behaviour is due to the fact that we have assumed

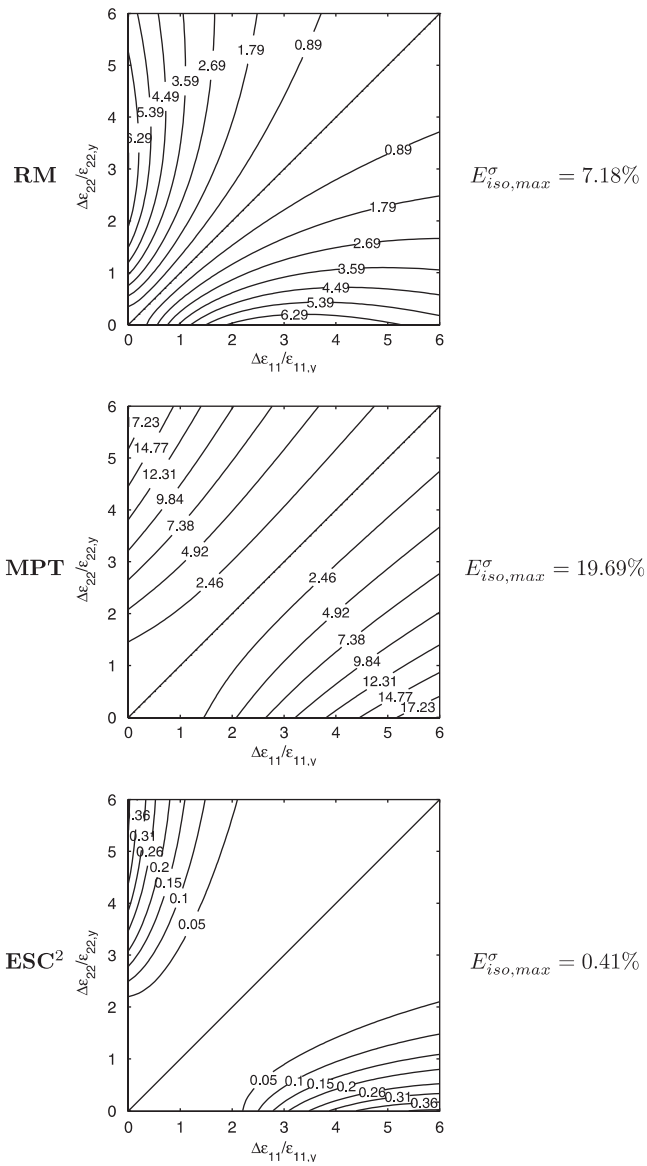

Figure 8. Comparison between return map (RM), midpoint (MPT) and the new exponential-based scheme (ESC^2). Iso-error maps for yield surface State 1—B and indication of the maximum stress error level.

a mixed stress–strain history and not a completely strain driven one. This interesting aspect is postponed to the discussion presented in Section 6.4.

Remark 6.2

It is noted that even with a non-zero value of isotropic hardening the ESC^2 scheme still produces more precise results for large time discretizations than both the RM and MPT scheme. The

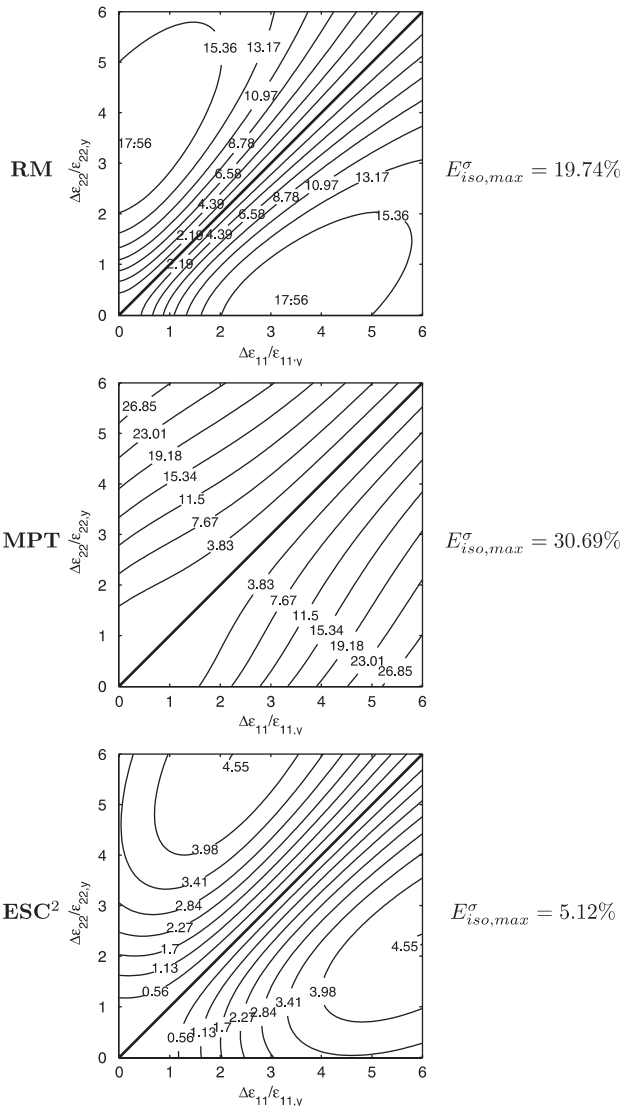

Figure 9. Comparison between return map (RM), midpoint (MPT) and the new exponential-based scheme (ESC^2). Iso-error maps for yield surface State 1—C and indication of the maximum stress error level.

reader is referred to Reference [23] where a wide set of iso-error maps regarding this particular case confirm the better performance of the exponential-based method.

6.3. Two initial boundary value problems

We consider two 3-dimensional thin rectangular perforated strips, subject to uniaxial extension in a plane strain state [3]. The first strip has a circular hole in the centre, while the second one

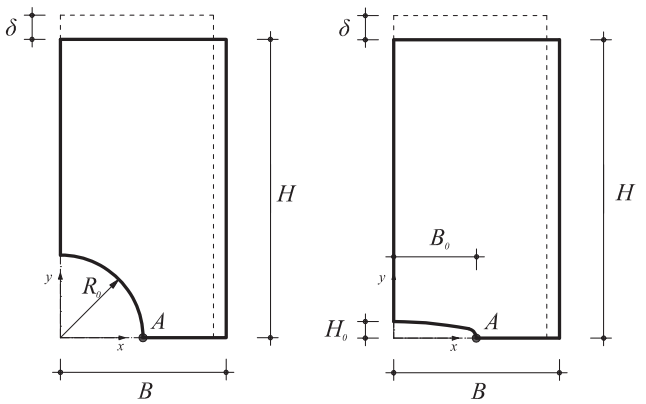

Figure 10. Boundary value problems. Strips with circular and elliptical holes: geometry and imposed displacements for a single quarter of the strips.

an elliptical hole. Both strips have three planes of symmetry and in Figure 10 we show one quarter of the domain for each of the two strips. The geometric lengths referred to Figure 10 are

$$B = 100\,\text{mm}, \quad H = 180\,\text{mm}, \quad R_0 = 50\,\text{mm}, \quad H_0 = 10\,\text{mm}, \quad B_0 = 50\,\text{mm}$$

while the thickness is 10 mm.

In the analysis we consider both Material 1 and Material 3, so that a total of four cases (two material sets for each strip) are investigated. The problem loading histories is composed of a first phase (1 s), in which, controlling the displacements, the strip is stretched assigning a top vertical displacement $\delta_{\max}$ and a second phase (1 s) in which the imposed displacement is set back to 0 mm. In the case of Material 1 we set $\delta_{\max} = 40\,\text{mm}$, while for Material 3 we set $\delta_{\max} = 5\,\text{mm}$. We solve the boundary value problems using the finite element code FEAP [20], in which we implemented the integration methods.

Due to geometry and loading symmetry, we solve the problem only on a quarter of the original domain (Figure 10), using 192 displacement-based SOLID2D [20] brick elements, as can be seen in Figure 11. As output, we count the number of residual evaluations per time step (i.e. number of Newton iterations per time step). The results are resumed in Tables III (Material 1) and IV (Material 3) in terms of the average number of iterations per step.

Since the algorithmically consistent tangent operator in the MPT scheme is not symmetric [6] we decided not to report its performance in the aforementioned tables, because the simulation would have actually involved a different solver for non-symmetric stiffness matrices.

As it can be seen the Newton convergence speeds of the exponential-based methods are similar and, by comparison, the return map needs around 15% fewer iterations to converge.

Finally, for both strips we monitor the displacement u^A of point A along the x direction (Figure 10), assuming that this is a good indicator on how the problem is actually approximated by the numerical methods. The comparison is carried out on the two linear converging methods, i.e. the RM and the ESC and the three quadratically accurate algorithms ENC, MPT, ESC^2. We compute the total modified relative error for the horizontal displacement at point A, between a discrete solution with variable number of steps and an 'exact' solution obtained with the

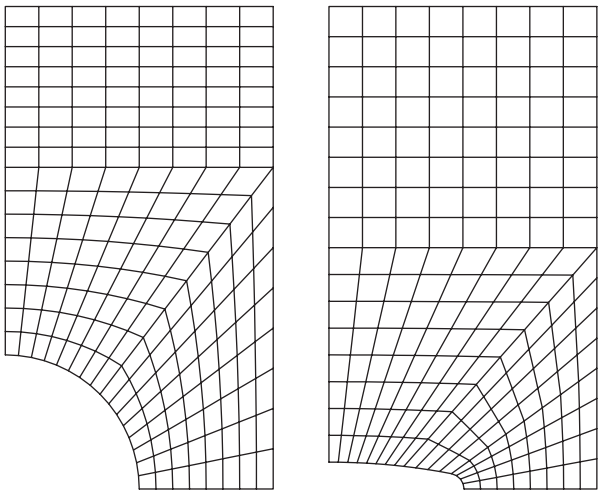

Figure 11. Boundary value problems. Strips with circular and elliptical holes: plane projection of the adopted meshes.

Table III. Boundary value problems for strips made of Material 1. Average number of iterations per time step as a function of time step size Δt.

	BVP 1			BVP 2		
	Δt (s)			Δt (s)		
Method	10^{-1}	10^{-2}	10^{-3}	10^{-1}	10^{-2}	10^{-3}
RM	3.25	2.83	2.73	3.65	3.18	2.95
ENN	4.30	3.17	2.91	4.85	3.70	3.33
ENC	4.30	3.17	2.90	4.70	3.66	3.27
ESC	4.30	3.17	2.90	4.70	3.66	3.27
ESC^2	4.55	3.24	2.91	4.75	3.66	3.27

Table IV. Boundary value problems for strips made of Material 3. Average number of iterations per time step as a function of time step size Δt.

	BVP 1			BVP 2		
	Δt (s)			Δt (s)		
Method	10^{-2}	10^{-3}	10^{-4}	10^{-2}	10^{-3}	10^{-4}
RM	4.90	4.28	3.68	5.00	4.33	3.75
ENN	7.18	4.96	4.28	7.71	5.17	4.45
ENC	7.21	4.97	4.30	7.72	5.16	4.42
ESC	7.21	4.97	4.30	7.72	5.16	4.42
ESC^2	7.22	4.87	4.30	7.65	5.16	4.41

Table V. Boundary value problems. Point A displacement total error versus number of steps per second.

	Steps/s	Total error RM ($\times 10^{-2}$)	Total error ESC ($\times 10^{-2}$)	Total error ENC ($\times 10^{-2}$)	Total error MPT ($\times 10^{-2}$)	Total error ESC^2 ($\times 10^{-2}$)
BVP 1—Mat. 1	10	6.21×10^{-2}	1.20×10^{-1}	1.28×10^{-1}	3.19×10^{-2}	3.34×10^{-2}
	20	4.37×10^{-2}	5.22×10^{-2}	2.92×10^{-2}	8.77×10^{-3}	8.03×10^{-3}
	40	2.46×10^{-2}	2.51×10^{-2}	7.86×10^{-3}	2.86×10^{-3}	2.65×10^{-3}
BVP 2—Mat. 1	10	4.18×10^{-1}	8.81×10^{-2}	2.28×10^{-1}	2.58×10^{-2}	5.58×10^{-2}
	20	2.08×10^{-1}	3.53×10^{-2}	5.68×10^{-2}	8.87×10^{-3}	1.53×10^{-2}
	40	1.04×10^{-1}	1.45×10^{-2}	1.36×10^{-2}	1.77×10^{-3}	3.41×10^{-3}

MPT with 1000 steps per second, i.e.

$$\tilde{E}_n^A = \sum_{n=1}^{N} \frac{|u_n^A - u_n^{A,\mathrm{ex}}|\Delta t}{\max_{j \in \{0,1,\ldots,n\}} |u_j^A|} \tag{151}$$

where u_n^A is the monitored displacement at time t_n calculated with the discrete method, while $u_n^{A,\mathrm{ex}}$ is the one obtained with the 'exact' solution.

For brevity's sake, the error measures reported in Table V refer only to strips made of Material 1. No significantly different results can in fact be deduced by the remaining problems.

As expected, Table V shows that the RM and ESC methods have linear convergence also in the global problem, while the ENC, MPT and ESC^2 keep their quadratic order of accuracy and result more accurate than the linear ones. Moreover, both the MPT and ESC^2 schemes produce smaller errors than the ENC method, the first two being almost comparable.

6.4. Piecewise linearity of the strain history and exactness of constitutive schemes in plasticity

Recalling that for plastic materials the stress response depends on the strain path, it is clear that, in the time-discrete framework, in order to be able to compute the stress some kind of assumption must be made on the evolution of the strain along each time interval. At the time-discrete level, the knowledge of the strain at the start and at the end of the step is not sufficient by itself to derive the stress response along each time interval. The most natural hypothesis is therefore to assume that the strain evolution is piecewise linear. A constitutive solver for plasticity can then be built starting from the strain driven asset and it can be implemented as part of a finite element method based for instance on a Newton–Raphson convergence strategy. The stress is then computed pointwise for each Gauss point of the mesh and at every integration instant t_n, $n = 0, 1, \ldots, N$.

On the other hand, the piecewise linear strain assumption is obviously false in general. As a consequence, the integration method carries an implicit 'strain path approximation error', which is in addition to any other error due to the constitutive law solution. In this sense, even methods which are 'exact', i.e. make no error for piecewise linear strain histories, will introduce some error in general plasticity problems. In particular this explains why the ESC^2 method, which is exact in the absence of isotropic hardening, is not completely error free in the iso-error maps

Table VI. Mixed stress–strain history.

Time (s)	$\boldsymbol{\varepsilon}_{11}$	$\boldsymbol{\varepsilon}_{22}$	σ_{33}	σ_{12}	σ_{13}	σ_{23}
$t=0$	0	0	0	0	0	0
$t=1$	$\varepsilon_{11,y}$	$\varepsilon_{22,y}$	0	0	0	0
$t=2$	$7\varepsilon_{11,y}$	$4\varepsilon_{22,y}$	0	0	0	0

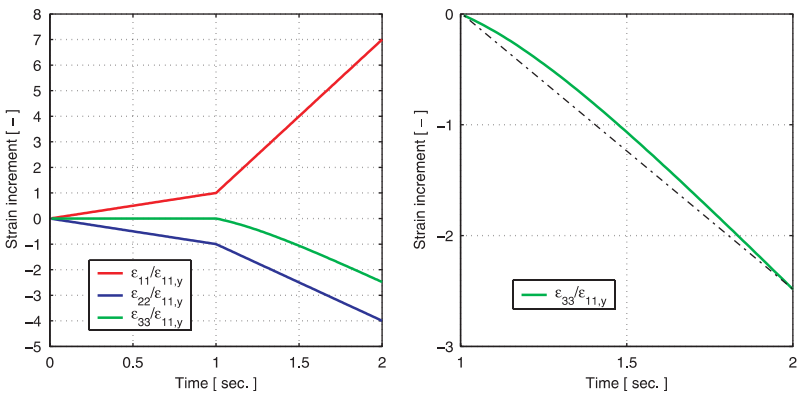

Figure 12. Mixed stress–strain history—evolution of $\boldsymbol{\varepsilon}_{11}$, $\boldsymbol{\varepsilon}_{22}$ and $\boldsymbol{\varepsilon}_{33}$ in time.

shown in Figures 7–9. This fact can also be appreciated considering the following pointwise mixed stress–strain problem adopting Material 2. The controlled quantities are

$$\varepsilon_{11} \quad \varepsilon_{22} \quad \sigma_{33} \quad \sigma_{12} \quad \sigma_{13} \quad \sigma_{23}$$

while the output is given by

$$\sigma_{11} \quad \sigma_{22} \quad \varepsilon_{33} \quad \varepsilon_{12} \quad \varepsilon_{13} \quad \varepsilon_{23}$$

The loading data is piecewise linear in time and described by the values shown in Table VI in terms of the following quantities:

$$\varepsilon_{11,y} = \frac{(1+\nu)}{3}\varepsilon_{\mathrm{y,mono}}, \quad \varepsilon_{22,\mathrm{y}} = -\frac{(1+\nu)}{3}\varepsilon_{\mathrm{y,mono}} \tag{152}$$

Note that at the end of the first time interval (i.e. $t=1$) the stress solution lays exactly on the yield surface and the plastic flow is zero. In other words, during the first half of this test the evolution is purely elastic as the stress simply moves from the origin to a particular point on the yield surface, representing a pure shear stress state. During the second half of the loading history, the material instead undergoes a plastic transformation.

The output components of stress and strain have been computed using the ESC[2] algorithm with a total of 200 uniform time steps. The result for the strain component $\boldsymbol{\varepsilon}_{33}$, which is not a loading data but a problem output, are shown in Figure 12. It is clear that the $\boldsymbol{\varepsilon}_{33}$ component is not linear in time in objection to the assumption made above on the strain.

7. CONCLUSIONS

We presented a new exponential-based algorithm (ESC^2) for the time-integration of a properly reformulated version of the von-Mises elasto-plastic constitutive model.

We have dedicated the first part of this note to the derivation of the new time continuous model and to the presentation of the integration algorithm. Then a detailed discussion on the numerical properties of the new procedure has been carried out. Differently from all the previous methods of the exponential-based family, the new one is both consistent and quadratically accurate. Regarding the convergence/stability results, some points are still to be addressed rigorously and this is demanded to the sequel of our work.

Finally, extensive numerical tests have been developed. In order to compare the new procedure with existing well established schemes, we have made use of two radial return map-type algorithms, respectively, the backward Euler integration scheme and the midpoint rule method. Also previously introduced exponential integration algorithms have been taken into account.

The pointwise tests show in general fairly higher precision in favour of the exponential methods, although on global finite element problems the Newton iteration convergence speed of the return-map-type methods seems slightly better. Another important feature arising from the tests is suggested by iso-error map plots: the ESC^2 method is the best-performing one for large strain increments in all the investigated cases.

When considering the von-Mises plasticity model, the exponential schemes seem therefore competitive with the classical return map algorithms. In particular such new methods couple the advantage of the Krieg and Krieg methods [13, 14], i.e. perform decisively better in the absence of isotropic hardening, with a larger range of applicability.

Clearly an important question, which is the application to different plasticity models, is still open; the authors are trustful that these same principles can be extended to other models.

APPENDIX A

In the following the reader is provided with the proofs of the lemmas recalled in Section 5.5 devoted to the numerical analysis of the exponential-based algorithms. Subsequently, we present a thorough derivation of the consistent tangent operator of the ESC^2 integration scheme.

A.1. Two lemmas

We now introduce and prove the two lemmas mentioned in the previous sections by first recalling the following identities which can be derived from the new formulation of Section 3. At all time instants during plastic steps it holds

$$\mathbf{X}^{\mathrm{s}} = \sigma_{\mathrm{y},0}^{-1} X_0^{1-q} \boldsymbol{\Sigma} \tag{A1}$$

$$\boldsymbol{\Sigma} = \sigma_{\mathrm{y},0} X_0^{q-1} \mathbf{X}^{\mathrm{s}} \tag{A2}$$

Lemma A.1

Let two initial couples $(\boldsymbol{\Sigma}(t_0), \sigma_{\mathrm{y}}(t_0))$, $(\tilde{\boldsymbol{\Sigma}}(t_0), \tilde{\sigma}_{\mathrm{y}}(t_0))$ and a strain increment $\Delta\mathbf{e} = \dot{\mathbf{e}}\Delta t$ be assigned. Assume to apply one step of the ESC or ESC^2 algorithm with strain increment $\Delta\mathbf{e}$

to both initial couples and assume that both steps are totally plastic. Then at all instants $t \in [t_0, t_0 + \Delta t]$ during the time step, it holds

$$\frac{\mathrm{d}}{\mathrm{d}t}|||\boldsymbol{\Sigma}(t) - \tilde{\boldsymbol{\Sigma}}(t), \sigma_{\mathrm{y}}(t) - \tilde{\sigma}_{\mathrm{y}}(t)|||$$

$$\leqslant \|\dot{\mathbf{e}}\|[K_1|||\boldsymbol{\Sigma}(t_0) - \tilde{\boldsymbol{\Sigma}}(t_0), \sigma_{\mathrm{y}}(t_0) - \tilde{\sigma}_{\mathrm{y}}(t_0)||| + K_2|||\boldsymbol{\Sigma}(t) - \tilde{\boldsymbol{\Sigma}}(t), \sigma_{\mathrm{y}}(t) - \tilde{\sigma}_{\mathrm{y}}(t)|||] \tag{A3}$$

where the positive constants K_1, K_2, depending only on the material constants and $\|\Delta\mathbf{e}\|$, are bounded on all sets of the type $\{\Delta\mathbf{e} \in \mathbb{R}^6,\ \|\Delta\mathbf{e}\| \leqslant c,\ c \in \mathbb{R}^+\}$.

Proof

The proof will be shown only in the case of the ESC^2 algorithm. The proof for the ESC scheme is a simpler version of the one that follows and can be trivially derived following the same steps. In the sequel, in order to shorten the notation, the dependence of the variables on time will not be explicited; unless differently noted, the time dependent equations and identities that follow are valid for all $t \in [t_0, t_0 + \Delta t]$.

We will again adopt the notation introduced in (125). Direct derivation gives

$$\frac{\mathrm{d}}{\mathrm{d}t}|||\boldsymbol{\Sigma}^E, \sigma_{\mathrm{y}}^E|||^2 = 2[(2G)^{-1}(\boldsymbol{\Sigma}^E, \dot{\boldsymbol{\Sigma}}^E) + (H_{\mathrm{iso}})^{-1}\sigma_{\mathrm{y}}^E \dot{\sigma}_{\mathrm{y}}^E] \tag{A4}$$

Deriving in time definition (A2) and using (24)–(A1) we easily get, without showing all the calculations

$$\dot{\boldsymbol{\Sigma}}^E = \frac{\mathrm{d}}{\mathrm{d}t}(\boldsymbol{\Sigma} - \tilde{\boldsymbol{\Sigma}}) = \sigma_{\mathrm{y},0}\mathbf{T}_1 + \mathbf{T}_2 \tag{A5}$$

$$\mathbf{T}_1 = \left[\frac{2G}{R}X_0^q - \frac{2G}{\tilde{R}}\tilde{X}_0^q\right]\dot{\mathbf{e}} \tag{A6}$$

$$\mathbf{T}_2 = (q-1)\left[\frac{2G}{R}(\dot{\mathbf{e}} \cdot \boldsymbol{\Sigma})\frac{\boldsymbol{\Sigma}}{\sigma_{\mathrm{y}}} - \frac{2G}{\tilde{R}}(\dot{\mathbf{e}} \cdot \tilde{\boldsymbol{\Sigma}})\frac{\tilde{\boldsymbol{\Sigma}}}{\tilde{\sigma}_{\mathrm{y}}}\right] \tag{A7}$$

As a consequence, the first member in the right-hand side of (A4) can be bounded with

$$(2G)^{-1}\boldsymbol{\Sigma}^E \cdot \dot{\boldsymbol{\Sigma}}^E = (2G)^{-1}[\sigma_{\mathrm{y},0}\mathbf{T}_1 + \mathbf{T}_2] \cdot \boldsymbol{\Sigma}^E \leqslant C(\|\mathbf{T}_1\| + \|\mathbf{T}_2\|)\|\boldsymbol{\Sigma}^E\| \tag{A8}$$

where here and in the sequel C indicates a general positive constant depending only on the material constants. We now have

$$\|\mathbf{T}_1\| \leqslant C\left|\frac{\tilde{R} - R}{R\tilde{R}}X_0^q + \frac{1}{\tilde{R}}(X_0^q - \tilde{X}_0^q)\right|\|\dot{\mathbf{e}}\|$$

$$\leqslant C\left(\left|\frac{\tilde{R} - R}{R\tilde{R}}X_0^q\right| + \left|\frac{1}{\tilde{R}}(X_0^q - \tilde{X}_0^q)\right|\right)\|\dot{\mathbf{e}}\| = (A_1 + A_2)\|\dot{\mathbf{e}}\| \tag{A9}$$

The definition of R, recalling that both couples are undergoing a purely plastic step, becomes

$$R = \frac{\|\boldsymbol{\Sigma}_i\|}{c^{-1}\ln(1+c)} \tag{A10}$$

$$c = \frac{2Gq\boldsymbol{\Sigma}_i \cdot \Delta\mathbf{e}}{\|\boldsymbol{\Sigma}_i\|^2} \tag{A11}$$

and the analogous for the bar variables. Therefore R is a real C^1 function of $\boldsymbol{\Sigma}_i$.

Recalling that both couples are in plastic phase, it follows immediately that both $\|\boldsymbol{\Sigma}_i\|$ and $\|\tilde{\boldsymbol{\Sigma}}_i\|$ are greater or equal to $\sigma_{y,0}$. It is therefore easy to check that there exists a smooth path $\boldsymbol{\gamma}$ in $\mathbb{R}^6$ from $\tilde{\boldsymbol{\Sigma}}_i$ to $\boldsymbol{\Sigma}_i$ such that

$$\boldsymbol{\gamma} : [0, L] \longrightarrow \mathbb{R}^6 \tag{A12}$$

$$\|\nabla\boldsymbol{\gamma}(s)\| = 1 \quad \forall s \in [0, L] \tag{A13}$$

$$\|\boldsymbol{\gamma}(s)\| \geqslant \sigma_{y,0} \quad \forall s \in [0, L] \tag{A14}$$

$$L \leqslant 4\|\boldsymbol{\Sigma}_i - \tilde{\boldsymbol{\Sigma}}_i\| \tag{A15}$$

Note that the above conditions simply mean that $\boldsymbol{\gamma}$ is a C^1 path of length L lesser than $4\|\boldsymbol{\Sigma}_i - \tilde{\boldsymbol{\Sigma}}_i\|$, written with respect to its curvilinear abscissae and bounded outside a sphere of radius $\sigma_{y,0}$ centred at the origin.

From the Lagrange theorem applied to the function $R(\boldsymbol{\Sigma})$ along the path $\boldsymbol{\gamma}$, it follows the existence of $\beta \in [0, L]$ such that

$$R - \tilde{R} = L\nabla R|_{\boldsymbol{\Sigma}_i^*} \cdot \nabla\boldsymbol{\gamma}|_\beta \tag{A16}$$

where

$$\boldsymbol{\Sigma}_i^* = \boldsymbol{\gamma}(\beta) \quad 0 \leqslant \beta \leqslant L \tag{A17}$$

Using (A13) and (A15), from (A16) we get

$$|R - \tilde{R}| \leqslant 4\|\nabla R|_{\boldsymbol{\Sigma}_i^*}\|\|\boldsymbol{\Sigma}_i - \tilde{\boldsymbol{\Sigma}}_i\| \tag{A18}$$

Substituting (A18) in the definition of A_1 and using the Cauchy–Schwartz inequality now leads to

$$A_1 \leqslant \frac{\|\nabla R|_{\boldsymbol{\Sigma}_i^*}\|}{\tilde{R}} \frac{X_0^q}{R}\|\boldsymbol{\Sigma}_i - \tilde{\boldsymbol{\Sigma}}_i\| \tag{A19}$$

We now want to bound the pieces in (A19). A direct calculation gives

$$\nabla R|_{\boldsymbol{\Sigma}_i^*} = \frac{1}{c^{-1}\ln(1+c)}\nabla\|\boldsymbol{\Sigma}\| - \|\boldsymbol{\Sigma}_i^*\| \frac{\dfrac{1}{c(1+c)} - \dfrac{\ln(1+c)}{c^2}}{(c^{-1}\ln(1+c))^2} \left[\frac{\partial c}{\partial \boldsymbol{\Sigma}}\right] \tag{A20}$$

where all the functions and derivatives are calculated in $\mathbf{\Sigma}_i^*$. We now note that the functions

$$\frac{1}{c(1+c)} - \frac{\ln(1+c)}{c^2}, \quad c^{-1}\ln(1+c) \tag{A21}$$

are bounded from above on all the positive real line. Also, recalling (A11), it is easy to check that the latter function $c^{-1}\ln(1+c)$ is bounded from below by a positive constant (independent of $\|\mathbf{\Sigma}_i^*\|$) on all sets of the type $\{\Delta\mathbf{e} \in \mathbb{R}^6,\ \|\Delta\mathbf{e}\| \leqslant c,\ c \in \mathbb{R}^+\}$. A direct calculation also easily gives

$$\left\| \left[\frac{\partial c}{\partial \mathbf{\Sigma}} \right] \Bigg|_{\mathbf{\Sigma}_i^*} \right\| \leqslant C \frac{\|\Delta\mathbf{e}\|}{\|\mathbf{\Sigma}_i^*\|^2} \tag{A22}$$

Joining the latter three statements with (A20) and noting that the norm of $\nabla(\|\mathbf{\Sigma}\|)$ is equal to one, gives

$$\|\nabla R|_{\mathbf{\Sigma}_i^*}\| \leqslant K_3'(1 + \|\mathbf{\Sigma}_i^*\|^{-1}) \tag{A23}$$

where K_3' depends only on $\|\Delta\mathbf{e}\|$ and is bounded on all sets of the type $\{\Delta\mathbf{e} \in \mathbb{R}^6,\ \|\Delta\mathbf{e}\| \leqslant c,\ c \in \mathbb{R}^+\}$. Finally, due to definition (A17) and condition (A14), the above bound becomes

$$\|\nabla R|_{\mathbf{\Sigma}_i^*}\| \leqslant K_3 \tag{A24}$$

where K_3 depends only on $\|\Delta\mathbf{e}\|$ and is bounded on all sets of the type $\{\Delta\mathbf{e} \in \mathbb{R}^6,\ \|\Delta\mathbf{e}\| \leqslant c,\ c \in \mathbb{R}^+\}$.

Using again the boundedness from above of $c^{-1}\ln(1+c)$ and recalling (A10), (55) we have

$$\frac{1}{\tilde{R}} \leqslant \frac{\tilde{c}^{-1}\ln(1+\tilde{c})}{\sigma_{\mathrm{y},0}} \leqslant C \tag{A25}$$

$$\frac{1}{R} = \frac{c^{-1}\ln(1+c)}{\sigma_{\mathrm{y},0} X_{0,i}^q} \leqslant C \frac{1}{X_{0,i}^q} \tag{A26}$$

Using (A26) and recalling that X_0 never decreases during the step, we now haver

$$\frac{X_0^q}{R} \leqslant C \left(\frac{X_0}{X_{0,i}} \right)^q \leqslant C \left(\frac{X_{0,f}}{X_{0,i}} \right)^q \tag{A27}$$

We now observe that, due to (43)–(44) and recalling that

$$\|\mathbf{X}^{\mathrm{s}}\| = X_0 \quad \text{during plastic phases} \tag{A28}$$

it follows

$$X_{0,f} = b\frac{\dot{\mathbf{e}} \cdot \mathbf{X}_i^{\mathrm{s}}}{\|\dot{\mathbf{e}}\|} + aX_{0,i} \leqslant b\|\mathbf{X}_i^{\mathrm{s}}\| + aX_{0,i} \leqslant (b+a)X_{0,i} \tag{A29}$$

Therefore, from (A27) and (A29), it follows

$$\frac{X_0^q}{R} \leqslant C(b+a)^q \leqslant C \exp\left(\frac{2Gq}{R}\|\Delta\mathbf{e}\|\right) \leqslant K_4 \tag{A30}$$

with K_4 bounded on all sets of the type $\{\Delta\mathbf{e} \in \mathbb{R}^6,\ \|\Delta\mathbf{e}\| \leqslant c,\ c \in \mathbb{R}^+\}$.

Finally, simply applying the three bounds (A24), (A25) and (A30) into (A19), we obtain

$$A_1 \leqslant K_5\|\boldsymbol{\Sigma}_i - \tilde{\boldsymbol{\Sigma}}_i\| \tag{A31}$$

with K_5 depending only on $\Delta\mathbf{e}$ and bounded on all sets of the type $\{\Delta\mathbf{e} \in \mathbb{R}^6,\ \|\Delta\mathbf{e}\| \leqslant c,\ c \in \mathbb{R}^+\}$. Using (A25) and observing that any difference of vector norms is bounded by the norm of the difference, we get for the second term in (A9)

$$A_2 = \left|\frac{1}{\tilde{R}}\sigma_{y,0}^{-1}(\|\boldsymbol{\Sigma}\| - \|\tilde{\boldsymbol{\Sigma}}\|)\right| \leqslant C(\|\boldsymbol{\Sigma}\| - \|\tilde{\boldsymbol{\Sigma}}\|) \leqslant C\|\boldsymbol{\Sigma} - \tilde{\boldsymbol{\Sigma}}\| \tag{A32}$$

Applying the bounds (A31) and (A32) to (A9), it immediately follows

$$\|\mathbf{T}_1\| \leqslant \|\dot{\mathbf{e}}\|[K_5\|\boldsymbol{\Sigma}_i - \tilde{\boldsymbol{\Sigma}}_i\| + C\|\boldsymbol{\Sigma} - \tilde{\boldsymbol{\Sigma}}\|] \tag{A33}$$

The second term $\mathbf{T}_2$ is bound following the same techniques; in the end we obtain a similar bound

$$\|\mathbf{T}_2\| \leqslant \|\dot{\mathbf{e}}\|[K_6\|\boldsymbol{\Sigma}_i - \tilde{\boldsymbol{\Sigma}}_i\| + K_7\|\boldsymbol{\Sigma} - \tilde{\boldsymbol{\Sigma}}\|] \tag{A34}$$

where K_6, K_7 depend only on $\|\Delta\mathbf{e}\|$ and are bounded on all sets of the type $\{\Delta\mathbf{e} \in \mathbb{R}^6,\ \|\Delta\mathbf{e}\| \leqslant c,\ c \in \mathbb{R}^+\}$.

For the second term in (A4), using the identities (55) and (28) it follows

$$|\sigma^E\dot{\sigma}^E| = |\sigma_y - \tilde{\sigma}_y|\sigma_{y,0}|X_0^{q-1}\dot{X}_0 - \tilde{X}_0^{q-1}\dot{\tilde{X}}_0| \tag{A35}$$

which, recalling that in plastic phase $\sigma_y = \|\boldsymbol{\Sigma}\|$, becomes

$$|\sigma^E\dot{\sigma}^E| \leqslant C\|\boldsymbol{\Sigma} - \tilde{\boldsymbol{\Sigma}}\|\sigma_{y,0}|X_0^{q-1}\dot{X}_0 - \tilde{X}_0^{q-1}\dot{\tilde{X}}_0| \tag{A36}$$

Applying identity (A1), bound (A36) becomes

$$|\sigma^E\dot{\sigma}^E| \leqslant C\|\boldsymbol{\Sigma} - \tilde{\boldsymbol{\Sigma}}\|\left(\frac{2G}{R}\dot{\mathbf{e}}\cdot\boldsymbol{\Sigma} - \frac{2G}{\tilde{R}}\dot{\mathbf{e}}\cdot\tilde{\boldsymbol{\Sigma}}\right) \tag{A37}$$

where the term in parentheses can be bounded with the usual techniques. We then get

$$|\sigma^E\dot{\sigma}^E| \leqslant \|\boldsymbol{\Sigma} - \tilde{\boldsymbol{\Sigma}}\|\|\dot{\mathbf{e}}\|[K_{10}\|\boldsymbol{\Sigma}_i - \tilde{\boldsymbol{\Sigma}}_i\| + K_{11}\|\boldsymbol{\Sigma} - \tilde{\boldsymbol{\Sigma}}\|] \tag{A38}$$

where K_{10}, K_{11} share the usual property of the previous cases.

Simply applying the four bounds (A8), (A33), (A34) and (A38) into (A4), we now obtain

$$\begin{aligned}\frac{\mathrm{d}}{\mathrm{d}t}|||\boldsymbol{\Sigma}^E(t), \sigma_y(t)^E|||^2 &\leqslant \|\dot{\mathbf{e}}\|[K_1\|\boldsymbol{\Sigma}_i - \tilde{\boldsymbol{\Sigma}}_i\| + K_2\|\boldsymbol{\Sigma} - \tilde{\boldsymbol{\Sigma}}\|]\|\boldsymbol{\Sigma}^E\| \\ &\leqslant C\|\dot{\mathbf{e}}\|[K_1\|\boldsymbol{\Sigma}_i - \tilde{\boldsymbol{\Sigma}}_i\| + K_2\|\boldsymbol{\Sigma} - \tilde{\boldsymbol{\Sigma}}\|]|||\boldsymbol{\Sigma}^E(t), \sigma_y(t)^E|||\end{aligned} \tag{A39}$$

where K_1, K_2 depend only on $\|\Delta\mathbf{e}\|$ and are bounded on all sets of the type $\{\Delta\mathbf{e} \in \mathbb{R}^6,\ \|\Delta\mathbf{e}\| \leqslant c,\ c \in \mathbb{R}^+\}$. Now observing that

$$\frac{\mathrm{d}}{\mathrm{d}t}|||\boldsymbol{\Sigma}^E(t), \sigma_{\mathrm{y}}(t)^E|||^2 = 2|||\boldsymbol{\Sigma}^E(t), \sigma_{\mathrm{y}}(t)^E|||\frac{\mathrm{d}}{\mathrm{d}t}|||\boldsymbol{\Sigma}^E(t), \sigma_{\mathrm{y}}(t)^E||| \tag{A40}$$

bound (A39) trivially proves the lemma. □

Lemma A.2
Let two initial couples $(\boldsymbol{\Sigma}(t_0), \sigma_{\mathrm{y}}(t_0))$, $(\tilde{\boldsymbol{\Sigma}}(t_0), \tilde{\sigma}_{\mathrm{y}}(t_0))$ and a strain increment $\Delta\mathbf{e} = \dot{\mathbf{e}}\Delta t$ be assigned. Assume to apply one step of the ESC algorithm with strain increment $\Delta\mathbf{e}$ to both initial couples; assume also that the step for the first couple is totally plastic, while the step for the second couple is totally elastic. Then at all instants $t \in [t_0, t_0 + \Delta t]$ during the time step, it holds

$$\begin{aligned}&\frac{\mathrm{d}}{\mathrm{d}t}|||\boldsymbol{\Sigma}(t) - \tilde{\boldsymbol{\Sigma}}(t), \sigma_{\mathrm{y}}(t) - \tilde{\sigma}_{\mathrm{y}}(t)|||\\ &\quad\leqslant \|\dot{\mathbf{e}}\|[K_1|||\boldsymbol{\Sigma}(t_0) - \tilde{\boldsymbol{\Sigma}}(t_0), \sigma_{\mathrm{y}}(t_0) - \tilde{\sigma}_{\mathrm{y}}(t_0)||| + K_2|||\boldsymbol{\Sigma}(t) - \tilde{\boldsymbol{\Sigma}}(t), \sigma_{\mathrm{y}}(t) - \tilde{\sigma}_{\mathrm{y}}(t)|||]\end{aligned} \tag{A41}$$

where the positive constants K_1, K_2 depend only on $\|\Delta\mathbf{e}\|$ and are bounded on all sets of the type $\{\Delta\mathbf{e} \in \mathbb{R}^6,\ \|\Delta\mathbf{e}\| \leqslant c,\ c \in \mathbb{R}^+\}$.

Proof
As in the proof of Lemma A.1 in the Appendix, the dependence of the variables on time will not be explicited. Unless differently noted, the time dependent equations and identities that follow are valid for all $t \in [t_0, t_0 + \Delta t]$.

We will again adopt the notation introduced in (125). Following the same identical initial steps as in Lemma 1, we get

$$\frac{\mathrm{d}}{\mathrm{d}t}|||\boldsymbol{\Sigma}^E, \sigma_{\mathrm{y}}^E|||^2 = 2[(2G)^{-1}\boldsymbol{\Sigma}^E \cdot \dot{\boldsymbol{\Sigma}}^E + (H_{\mathrm{iso}})^{-1}\sigma_{\mathrm{y}}^E\dot{\sigma}_{\mathrm{y}}] \tag{A42}$$

where we implicitly used that $\dot{\sigma}_{\mathrm{y}}^E = \dot{\sigma}_{\mathrm{y}}$ because the second couple is in elastic phase. Note that for the time derivative of $\tilde{\mathbf{X}}$, which is in elastic phase, it holds

$$\frac{\mathrm{d}}{\mathrm{d}t}\tilde{\mathbf{X}}^{\mathrm{s}} = \frac{2G}{\sigma_{\mathrm{y},i}}\tilde{X}_0\dot{\mathbf{e}} \tag{A43}$$

$$\frac{\mathrm{d}}{\mathrm{d}t}\tilde{X}_0 = 0 \tag{A44}$$

while the time derivative of $\mathbf{X}$ still follows (24)–(A1). Deriving in time definition (A2), then using (24)–(A1) and (A43)–(A44), we easily get, without showing all the calculations

$$\dot{\boldsymbol{\Sigma}}^E = \frac{\mathrm{d}}{\mathrm{d}t}(\boldsymbol{\Sigma} - \tilde{\boldsymbol{\Sigma}}) = \sigma_{\mathrm{y},0}\mathbf{T}_1 + \mathbf{T}_2 \tag{A45}$$

$$\mathbf{T}_1 = \left[\frac{2G}{\sigma_{\mathrm{y},i}} X_0^q - \frac{2G}{\tilde{\sigma}_{\mathrm{y},i}} \tilde{X}_0^q\right] \dot{\mathbf{e}} \tag{A46}$$

$$\mathbf{T}_2 = (q-1)\left[\frac{2G}{R}(\dot{\mathbf{e}} \cdot \boldsymbol{\Sigma})\frac{\boldsymbol{\Sigma}}{\sigma_{\mathrm{y}}}\right] \tag{A47}$$

Joining (A42) and (A45) gives

$$\begin{aligned}\frac{\mathrm{d}}{\mathrm{d}t}|||\boldsymbol{\Sigma}^E, \sigma_{\mathrm{y}}^E|||^2 &= 2(2G)^{-1}\sigma_{\mathrm{y},0}\mathbf{T}_1 \cdot \boldsymbol{\Sigma}^E + 2[(2G)^{-1}\mathbf{T}_2 \cdot \boldsymbol{\Sigma}^E + (H_{\mathrm{iso}})^{-1}\sigma_{\mathrm{y}}^E \dot{\sigma}_{\mathrm{y}}] \\ &=: A_1 + A_2 \end{aligned} \tag{A48}$$

Recalling the identity (55), which holds in all phases and using that $\tilde{\sigma}_{\mathrm{y}} = \tilde{\sigma}_{\mathrm{y},i}$ during all the step, we get

$$A_1 = 2\left(\frac{\sigma_{\mathrm{y}}}{\sigma_{\mathrm{y},i}} - 1\right)\dot{\mathbf{e}} \cdot \boldsymbol{\Sigma}^E \leqslant \frac{2}{\sigma_{\mathrm{y},i}}|\sigma_{\mathrm{y}} - \sigma_{\mathrm{y},i}|\|\boldsymbol{\Sigma}^E\|\|\dot{\mathbf{e}}\| \tag{A49}$$

Observing that $\sigma_{\mathrm{y},i} \geqslant \sigma_{\mathrm{y},0}$ and $\tilde{\sigma}_{\mathrm{y}} = \tilde{\sigma}_{\mathrm{y},i}$, due to a triangle inequality it follows

$$A_1 \leqslant \frac{2}{\sigma_{\mathrm{y},0}}(|\sigma_{\mathrm{y}} - \tilde{\sigma}_{\mathrm{y}}| + |\sigma_{\mathrm{y},i} - \tilde{\sigma}_{\mathrm{y},i}|)\|\boldsymbol{\Sigma}^E\|\|\dot{\mathbf{e}}\| \tag{A50}$$

which, from definition (123), becomes

$$A_1 \leqslant C(|||\boldsymbol{\Sigma}_i^E, \sigma_{\mathrm{y},i}^E||| + |||\boldsymbol{\Sigma}^E, \sigma_{\mathrm{y}}^E|||)|||\boldsymbol{\Sigma}^E, \sigma_{\mathrm{y}}^E||||\dot{\mathbf{e}}\| \tag{A51}$$

where the scalar C depends only on the material constants.

Deriving in time and applying (28) we now get

$$\dot{\sigma}_{\mathrm{y}} = \frac{\mathrm{d}}{\mathrm{d}t}[\sigma_{\mathrm{y},0}X_0^q] = q\sigma_{\mathrm{y},0}X_0^{q-1}\dot{X}_0 = q\sigma_{\mathrm{y},0}X_0^{q-1}\frac{2G}{\sigma_{\mathrm{y},i}}\dot{\mathbf{e}} \cdot \mathbf{X}^{\mathrm{s}} \tag{A52}$$

Applying (55) and (A1), the identity above easily gives

$$\dot{\sigma}_{\mathrm{y}} = q\frac{2G}{\sigma_{\mathrm{y},i}}\dot{\mathbf{e}} \cdot \boldsymbol{\Sigma} \tag{A53}$$

From the definition of q (see (55)), identity (A53) and rearranging the terms, the second member in (A48) becomes

$$\begin{aligned} A_2 &= \left[-2\frac{2G}{2G + H_{\mathrm{iso}}}\frac{\boldsymbol{\Sigma}}{\sigma_{\mathrm{y}}} \cdot \boldsymbol{\Sigma}^E + 2\frac{2G}{2G + H_{\mathrm{iso}}}\sigma_{\mathrm{y}}^E\right]\frac{\dot{\mathbf{e}} \cdot \boldsymbol{\Sigma}}{\sigma_{\mathrm{y},i}} \\ &= 2\frac{2G}{2G + H_{\mathrm{iso}}}\left[-\frac{\boldsymbol{\Sigma}}{\sigma_{\mathrm{y}}} \cdot \boldsymbol{\Sigma}^E + \sigma_{\mathrm{y}} - \tilde{\sigma}_{\mathrm{y}}\right]\frac{\dot{\mathbf{e}} \cdot \boldsymbol{\Sigma}}{\sigma_{\mathrm{y},i}} \end{aligned} \tag{A54}$$

which we will show being lesser or equal than zero. Note that, being the first couple in purely plastic phase, $\dot{\mathbf{e}} \cdot \boldsymbol{\Sigma} \geqslant 0$; as a consequence, in order to show

$$A_2 \leqslant 0 \tag{A55}$$

it is sufficient to show

$$-\frac{\boldsymbol{\Sigma}}{\sigma_y} \cdot \boldsymbol{\Sigma}^E + \sigma_y - \tilde{\sigma}_y \leqslant 0 \tag{A56}$$

Multiplying and dividing by σ_y, then recalling that $\|\boldsymbol{\Sigma}\| = \sigma_y$, we get

$$-\frac{\boldsymbol{\Sigma}}{\sigma_y} \cdot \boldsymbol{\Sigma}^E + \sigma_y - \tilde{\sigma}_y = \frac{1}{\sigma_y}[-\|\boldsymbol{\Sigma}\|^2 + \boldsymbol{\Sigma} \cdot \tilde{\boldsymbol{\Sigma}} + \sigma_y^2 - \sigma_y \tilde{\sigma}_y] \tag{A57}$$

$$= \frac{1}{\sigma_y}[\boldsymbol{\Sigma} \cdot \tilde{\boldsymbol{\Sigma}} - \sigma_y \tilde{\sigma}_y] \tag{A58}$$

A Cauchy–Schwarz inequality and the Kuhn–Tucker conditions applied to (A57) then give

$$-\frac{\boldsymbol{\Sigma}}{\sigma_y} \cdot \boldsymbol{\Sigma}^E + \sigma_y - \tilde{\sigma}_y \leqslant \frac{1}{\sigma_y}[\|\boldsymbol{\Sigma}\|\|\tilde{\boldsymbol{\Sigma}}\| - \sigma_y \tilde{\sigma}_y] \leqslant 0 \tag{A59}$$

which implies (A55). Joining (A51) and (A55) with (A48) implies

$$\frac{\mathrm{d}}{\mathrm{d}t}|||\boldsymbol{\Sigma}^E, \sigma_y^E|||^2 \leqslant C(|||\boldsymbol{\Sigma}_i^E, \sigma_{y,i}^E||| + |||\boldsymbol{\Sigma}^E, \sigma_y^E|||)|||\boldsymbol{\Sigma}^E, \sigma_y^E||||\dot{\mathbf{e}}\| \tag{A60}$$

which recalling (A40) easily proves the lemma. □

A.2. Tangent matrix for the generalized stress

In the following we present the tangent matrix of the *generalized stress vector* addressed in (66), which regards the new optimal exponential-based ESC^2 integration scheme. For what concerns the ESC scheme, the reader is referred to Reference [2] where a complete derivation of its tangent operator is developed. As it will be clear in the following, the tangent moduli operator corresponding to the ESC algorithm can be obtained in a straightforward manner by simply cancelling the $\mathbb{A}_5$ and $\mathbf{e}_5$ terms arising in the new discrete formulation. We now present the tangent matrix $\partial \mathbf{X}^s / \partial \mathbf{e}$ and tangent vector $\partial X_0 / \partial \mathbf{e}$ for plastic phases, which, from Equation (63), provide the tangent matrix $\partial \boldsymbol{\sigma} / \partial \boldsymbol{\varepsilon}$ of the new algorithm during plastic or mixed elasto-plastic steps. As usual, unless explicitly specified all relevant quantities are evaluated at the actual time step end, i.e. at t_{n+1}.

Recalling that purely plastic steps are a particular case within the range of mixed ones (see Section 4), we start analysing the latter. From (53)–(54), we have

$$\mathbf{X}_{n+1} = \bar{\mathbb{G}}_p \bar{\mathbb{G}}_e \mathbf{X}_n = \mathbb{G}_p[(1-\alpha)\Delta\mathbf{e}, R_n]\mathbb{G}_e[\alpha\Delta\mathbf{e}]\mathbf{X}_n \tag{A61}$$

where the above matrices are given by (44) and α (which depends on $\Delta\mathbf{e}$) is the 'elastic step proportion' defined in (51). Consequently, following basic differentiation rules, we have

$$\frac{\partial \mathbf{X}_{n+1}}{\partial \Delta\mathbf{e}} = [\tilde{\mathbb{A}}_1 + \tilde{\mathbb{A}}_2 + \tilde{\mathbb{A}}_3 + \tilde{\mathbb{A}}_4 + \tilde{\mathbb{A}}_5]\mathbf{X}_n \tag{A62}$$

with

$$\tilde{\mathbb{A}}_1 = \frac{\partial \bar{\mathbb{G}}_\mathrm{p}}{\partial \Delta\mathbf{e}}[(1-\alpha)\Delta\mathbf{e},\, R_n]\bar{\mathbb{G}}_\mathrm{e}[\alpha\Delta\mathbf{e}]$$

$$\tilde{\mathbb{A}}_2 = \frac{\partial \bar{\mathbb{G}}_\mathrm{p}}{\partial \alpha}[(1-\alpha)\Delta\mathbf{e},\, R_n]\frac{\mathrm{d}\alpha}{\mathrm{d}\Delta\mathbf{e}}[\Delta\mathbf{e}]\bar{\mathbb{G}}_\mathrm{e}[\alpha\Delta\mathbf{e}]$$

$$\tilde{\mathbb{A}}_3 = \bar{\mathbb{G}}_\mathrm{p}[(1-\alpha)\Delta\mathbf{e},\, R_n]\frac{\partial \bar{\mathbb{G}}_\mathrm{e}}{\partial \Delta\mathbf{e}}[\alpha\Delta\mathbf{e}] \tag{A63}$$

$$\tilde{\mathbb{A}}_4 = \bar{\mathbb{G}}_\mathrm{p}[(1-\alpha)\Delta\mathbf{e},\, R_n]\frac{\partial \bar{\mathbb{G}}_\mathrm{e}}{\partial \alpha}[\alpha\Delta\mathbf{e}]\frac{\mathrm{d}\alpha}{\mathrm{d}\Delta\mathbf{e}}[\Delta\mathbf{e}]$$

$$\tilde{\mathbb{A}}_5 = \frac{\partial \bar{\mathbb{G}}_\mathrm{p}}{\partial R_n}[(1-\alpha)\Delta\mathbf{e},\, R_n]\frac{\partial R_n}{\partial \Delta\mathbf{e}}[\Delta\mathbf{e},\, \sigma_{\mathrm{y},n}]\bar{\mathbb{G}}_\mathrm{e}[\alpha\Delta\mathbf{e}]$$

From Equation (A62) we can immediately derive $\partial\mathbf{X}^\mathrm{s}_{n+1}/\partial\mathbf{e}$ (first 6 components) and $\partial\mathbf{X}_{0,n+1}/\partial\mathbf{e}$ (last component); in order to obtain the classical tangent matrix, the obtained equations must be finally expressed as a linear function of the strain derivation vector instead of in the form (A62), which is expressed as a linear function of $\mathbf{X}_n$. Doing so, we finally obtain that for mixed steps

$$\frac{\partial\mathbf{X}^\mathrm{s}}{\partial\mathbf{e}} = \mathbb{A}_1 + \mathbb{A}_2 + \mathbb{A}_3 + \mathbb{A}_4 + \mathbb{A}_5 \tag{A64}$$

$$\frac{\partial\mathbf{X}_0}{\partial\mathbf{e}} = \mathbf{b}_1 + \mathbf{b}_2 + \mathbf{b}_3 + \mathbf{b}_4 + \mathbf{b}_5 \tag{A65}$$

where the matrices $\mathbb{A}$ and vectors $\mathbf{b}$ are described below without addressing the calculations. For purely plastic steps, being α constantly equal to zero, we instead obtain the shorter formulation

$$\frac{\partial\mathbf{X}^\mathrm{s}}{\partial\mathbf{e}} = \mathbb{A}_1 \tag{A66}$$

$$\frac{\partial\mathbf{X}_0}{\partial\mathbf{e}} = \mathbf{b}_1 \tag{A67}$$

We start introducing (see again (51) for M, D, C in each step) the vector $\boldsymbol{\upsilon} = \mathrm{d}\alpha/\mathrm{d}\Delta\mathbf{e}$

$$\boldsymbol{\upsilon} = \phi_1\frac{\mathrm{d}C}{\mathrm{d}\Delta\mathbf{e}} + \phi_2\frac{\mathrm{d}D}{\mathrm{d}\Delta\mathbf{e}}$$

$$\phi_1 = \frac{1}{D}\left(\frac{C}{\sqrt{C^2 - DM}} - 1\right)$$

$$\phi_2 = -\frac{1}{D^2}\left(\frac{DM}{2\sqrt{C^2 - DM}} + \sqrt{C^2 - DM} - C\right)$$

$$\begin{aligned}\frac{\mathrm{d}C}{\mathrm{d}\Delta\mathbf{e}} &= \frac{2G}{\sigma_{\mathrm{y},n}} X_{0,n} \mathbf{X}_n^{\mathrm{s}} \\ \frac{\mathrm{d}D}{\mathrm{d}\Delta\mathbf{e}} &= 2\left(\frac{2G}{\sigma_{\mathrm{y},n}} X_{0,n}\right)^2 \Delta\mathbf{e}\end{aligned} \tag{A68}$$

and the vector $\mathbf{w}$

$$\begin{aligned}\mathbf{w} &= p(\mathbf{w}_1 + \mathbf{w}_2) \\ p &= \frac{-\sigma_{\mathrm{y},n}}{[c^{-1}\ln(1+c)]^2}\left[\frac{1}{c(1+c)} - \frac{\ln(1+c)}{c^2}\right] \\ p_1 &= \frac{2Gq}{\sigma_{\mathrm{y},n}}(\Delta\mathbf{e}\cdot\mathbf{X}_n^{\mathrm{s}}) \\ p_2 &= \left(\frac{2G}{\sigma_{\mathrm{y},n}}\right)^2 q(1-\alpha)\|\Delta\mathbf{e}\|^2 \\ \mathbf{w}_1 &= (1-\alpha)\frac{2Gq}{\sigma_{\mathrm{y},n}}\mathbf{X}_n^{\mathrm{s}} - p_1\boldsymbol{\upsilon} \\ \mathbf{w}_2 &= p_2\boldsymbol{\upsilon} + \left(\frac{2G}{\sigma_{\mathrm{y},n}}\right)^2 q(1-\alpha)\Delta\mathbf{e}\end{aligned} \tag{A69}$$

Introducing the scalars

$$\begin{aligned}a &= \cosh\left(\frac{2G}{R}(1-\alpha)\|\Delta\mathbf{e}\|\right) \\ b &= \sinh\left(\frac{2G}{R}(1-\alpha)\|\Delta\mathbf{e}\|\right) \\ s &= \frac{\Delta\mathbf{e}\cdot\mathbf{X}_n^{\mathrm{s}}}{\|\Delta\mathbf{e}\|} \\ k &= \frac{2G}{R}(1-\alpha) \\ \tilde{k} &= -\frac{2G}{R}\|\Delta\mathbf{e}\|\end{aligned} \tag{A70}$$

and the matrices

$$\mathbb{M}_1 = s\left(kb - 2\frac{a-1}{\|\Delta\mathbf{e}\|}\right)\left[\frac{\Delta\mathbf{e}\Delta\mathbf{e}^{\mathrm{T}}}{\|\Delta\mathbf{e}\|^2}\right] + \frac{(a-1)s}{\|\Delta\mathbf{e}\|}\mathbb{I} + \frac{a-1}{\|\Delta\mathbf{e}\|}\left[\frac{\Delta\mathbf{e}\mathbf{X}_n^{\mathrm{s}\mathrm{T}}}{\|\Delta\mathbf{e}\|}\right] \tag{A71}$$

$$\mathbb{M}_2 = \left(ka - \frac{b}{\|\Delta\mathbf{e}\|}\right)\left[\frac{\Delta\mathbf{e}\Delta\mathbf{e}^{\mathrm{T}}}{\|\Delta\mathbf{e}\|^2}\right] + \frac{b}{\|\Delta\mathbf{e}\|}\mathbb{I} \tag{A72}$$

We can show that the matrices in (A64) are

$$\begin{aligned}
\mathbb{A}_1 &= \mathbb{M}_1 + X_{0,n}\mathbb{M}_2 \\
\mathbb{A}_2 &= \tilde{k}(bs + aX_{0,n}) \left[\frac{\Delta\mathbf{e}\boldsymbol{\upsilon}^{\mathrm{T}}}{\|\Delta\mathbf{e}\|} \right] \\
\mathbb{A}_3 &= \frac{2G}{R}\alpha X_{0,n} \left[\mathbb{I} + (a-1)\frac{\Delta\mathbf{e}\Delta\mathbf{e}^{\mathrm{T}}}{\|\Delta\mathbf{e}\|^2} \right] \\
\mathbb{A}_4 &= \frac{2G}{R} a X_{0,n} [\Delta\mathbf{e}\boldsymbol{\upsilon}^{\mathrm{T}}] \\
\mathbb{A}_5 &= -\frac{k}{R}\left(\frac{bs}{\|\Delta\mathbf{e}\|^2} + a \right) [\Delta\mathbf{e}\mathbf{w}^{\mathrm{T}}]
\end{aligned} \tag{A73}$$

while the row vectors in (A65) are

$$\begin{aligned}
\mathbf{b}_1 &= \mathbf{X}_n^{\mathrm{sT}}\mathbb{M}_2 + kbX_{0,n}\frac{\Delta\mathbf{e}^{\mathrm{T}}}{\|\Delta\mathbf{e}\|} \\
\mathbf{b}_2 &= \tilde{k}(as + bX_{0,n})\boldsymbol{\upsilon}^{\mathrm{T}} \\
\mathbf{b}_3 &= \frac{2G}{R}\alpha b X_{0,n}\frac{\Delta\mathbf{e}^{\mathrm{T}}}{\|\Delta\mathbf{e}\|} \\
\mathbf{b}_4 &= \frac{2G}{R} b X_{0,n}\|\Delta\mathbf{e}\|\boldsymbol{\upsilon}^{\mathrm{T}} \\
\mathbf{b}_5 &= -\frac{k}{R}\left(\frac{as}{\|\Delta\mathbf{e}\|} + b\|\Delta\mathbf{e}\| \right)\mathbf{w}^{\mathrm{T}}
\end{aligned} \tag{A74}$$

where a column vector after a matrix, or a row vector before, represents a matrix–vector product as usual.

REFERENCES

1. Auricchio F, Beirao da Veiga L. On a new integration scheme for von-Mises plasticity with linear hardening. *International Journal for Numerical Methods for Engineering* 2003; **56**:1375–1396.
2. Artioli E, Auricchio F, Beirao da Veiga L. Integration schemes for von-Mises plasticity models based on exponential maps: numerical investigations and theoretical considerations. *International Journal for Numerical Methods for Engineering* 2005; **64**:1133–1165.
3. Simo JC, Hughes TJR. *Computational Inelasticity*. Springer: Berlin, 1998.
4. Simo JC. Topics on the numerical analysis and simulation of plasticity. In *Handbook of Numerical Analysis*, Ciarlet PG, Lions JL (eds), vol. III. Elsevier Science Publisher B.V.: Amsterdam, 1999.
5. Zienkiewicz OC, Taylor RL. *The Finite Element Method*, vol. II (5th edn). McGraw-Hill: New York, 2002.
6. Ortiz M, Popov EP. Accuracy and stability of integration algorithms for elastoplastic constitutive relations. *International Journal for Numerical Methods for Engineering* 1985; **21**:1561–1576.
7. Chaboche JL. Constitutive equations for cyclic plasticity and cyclic visco-plasticity. *International Journal of Plasticity* 1989; **5**:247–302.
8. Lubliner J. *Plasticity Theory*. Macmillan: New York, 1990.

9. Han W, Reddy BD. *Plasticity*: *Mathematical Theory and Numerical Analysis*. Springer: Berlin, 1999.
10. Artioli E, Auricchio F, Beirao da Veiga L. A new integration scheme for von-Mises plasticity: numerical investigations. In *Proceedings XV Italian Conference on Computational Mechanics*, Genova, 21–23 June, 2004.
11. Hong-Ki Hong, Chien-Shan Liu. Internal symmetry in bilinear elastoplasticity. *International Journal of Non-Linear Mechanics* 1999; **34**:279–288.
12. Hong-Ki Hong, Chien-Shan Liu. Internal symmetry in the constitutive model of perfect elastoplasticity. *International Journal of Non-Linear Mechanics* 2000; **35**:447–466.
13. Krieg RD, Krieg DB. Accuracies of numerical solution methods for the elastic-perfectly plastic model. *Journal of Pressure Vessel Technology*, *Transaction of ASME* 1977; **99**:510–515.
14. Yoder PJ, Whirley RG. On the numerical implementation of elastoplastic models. *Journal of Applied Mechanics* 1984; **51**:283–288.
15. Ristinmaa M, Tryding J. Exact integration of constitutive equations in elasto-plasticity. *International Journal for Numerical Methods in Engineering* 1993; **36**:2525–2544.
16. Hairer E, Norsett SP, Wanner G. *Solving Ordinary Differential Equations I: Nonstiff Problems*. Springer: Berlin, 1987.
17. Lambert JD. *Computational Methods in Ordinary Differential Equations*. Wiley: Chichester, 1991.
18. Simo JC, Govindjee S. Non-linear B-stability and symmetry preserving return mapping algorithms for plasticity and visco-plasticity. *International Journal for Numerical Methods in Engineering* 1991; **31**:151.
19. Auricchio F. Ce-driver. *Technical Report*, Dipartimento di Meccanica Strutturale—University of Pavia, 2001. Manual prepared for the European School of Advanced Studies of Seismic Risk Reduction.
20. Taylor RL. A finite-element analysis program. *Technical Report*, University of California at Berkeley, 2000. http://www.ce.berkeley.edu/rlt.
21. Auricchio F, Taylor RL. Two material models for cyclic plasticity: Nonlinear kinematic hardening and generalized plasticity. *International Journal for Plasticity* 1995; **11**:65–98.
22. Ortiz M, Simo JC. An analysis of a new class of integration algorithms for elastoplastic constitutive relations. *International Journal for Numerical Methods for Engineering* 1986; **23**:353–366.
23. Artioli E, Auricchio F, Beirao da Veiga L. A new integration algorithm for the von-Mises elasto-plastic model. In *Proceedings Colloquium Lagrangianum*, Venice, 21–23 December, 2004.

